Available online at www.sciencedirect.com
SCIENCE DIRECT®
Advanced Drug Delivery Reviews 56 (2004) 145–172
Advanced DRUG DELIVERY Reviews
www.elsevier.com/locate/addr

Hard and soft micromachining for BioMEMS: review of techniques and examples of applications in microfluidics and drug delivery

Babak Ziaie[a,b], Antonio Baldi[a], Ming Lei[a], Yuandong Gu[c], Ronald A. Siegel[b,c,d,*]

[a] *Department of Electrical and Computer Engineering, University of Minnesota, Minneapolis, MN 55455, USA*
[b] *Biomedical Engineering Institute, University of Minnesota, Minneapolis, MN 55455, USA*
[c] *Department of Pharmaceutics, University of Minnesota, Minneapolis, MN 55455, USA*
[d] *Department of Biomedical Engineering, University of Minnesota,Minneapolis, MN 55455, USA*

Received 10 January 2003; accepted 1 September 2003

Abstract

Recent development in microfabrication (micromachining, microelectromechanical systems, MEMS) permits the integration of hard and soft structures, and enables the design of controllable microfluidic systems, which may be applied to drug delivery. In this paper, we present a tutorial review of both classical "hard" and more recent "soft" micromachining techniques. We then provide examples where these techniques are combined to produce hydrogel-based microfluidic control systems. The most complex of these systems utilizes a very small hydrogel based on phenylboronic acid to control the flow of an insulin solution in response to changes in glucose concentration.
© 2003 Elsevier B.V. All rights reserved.

Keywords: Closed-loop insulin delivery; MEMS; Microfluidics; Phenylboronic acid; Hydrogels; Glucose-sensitive

Contents

* Corresponding author. Department of Pharmaceutics, 9-177 Weaver-Densford Hall, University of Minnesota, 308 Harvard St. S.E., Minneapolis, MN 55455, USA. Tel.: +1-612-624-6164; fax: +1-612-626-2125.
E-mail address: siege017@umn.edu (R.A. Siegel).

0169-409X/$ - see front matter © 2003 Elsevier B.V. All rights reserved.
doi:10.1016/j.addr.2003.09.001

1. Background

Recent advances in micromachining, microelectromechanical systems (MEMS), and microsystem technology have provided a unique opportunity to fabricate miniature biomedical devices for a variety of applications ranging from implantable drug delivery systems and lab-on-a-chip to neural prosthetics [1–3]. These systems offer several major advantages as compared to other devices fabricated using traditional manufacturing techniques. These include: (1) smaller dimensions, (2) lower cost due to batch fabrication, (3) the ability to incorporate sensing, signal conditioning, and actuating functions in close proximity or on the same substrate, (4) superior functionality (resolution, sensitivity, etc.), and (5) the ability to provide redundancy and hence enhance the reliability by using numerous miniature devices.

Traditionally, silicon and glass have been the two major materials used in the micromachining and MEMS. These materials show superior mechanical properties which make them suitable for a variety of transducing applications (accelerometers, gyroscopes, etc.). However, many biomedical devices require alternative soft or polymeric materials such as silicone rubber, polycarbonate, isobornyl acrylate, and polyimide [4]. Polymers are inexpensive and can be used in disposable devices, relaxing stringent sterilization-upon-reuse requirements. In addition, polymers provide a more suitable interface with biological tissue, reducing irritation and scarring. Finally, polymers can exist in either a hard, glassy state or a soft, rubbery state, a variety that is not present in MEMS structures based on silicon or glass.

Incorporation of hydrogels, especially those whose swelling responds to changes in the external environment (e.g. temperature, pH, glucose level) into MEMS, is a recent development. Integration of such soft, responsive materials with micromachined hard and soft materials may lead to devices with environmentally responsive functionalities that are difficult to achieve with hard or soft components alone.

Most of the activities in the biomedical MEMS (BioMEMS) area in the 1990s were concentrated in the academia, but we are witnessing a move towards commercialization of many BioMEMS devices and systems. For example, a MEMS-based DNA sequencer (Smart Cycler®) developed by the Cepheid is currently being installed in post offices across the country for Bio-agent detection [5]. Bio-MEMS drug delivery systems are also actively targeted by many investigators and companies as is evident, for example, from current efforts by MicroCHIPS, to commercialize an electronically activated drug delivery microchip [6], by ChipRx, to introduce systems that integrate silicon and electroactive polymer technologies for controlled delivery [7], and iMEDD, to develop nanoporous membranes and micromachined particles for a variety of drug delivery applications [8].

Two major impediments to successful commercialization of Bio-MEMS devices have been testing and packaging. It is estimated that packaging constitutes of up to 80% of the device final cost. Packaging is a particularly challenging task if the device is to be implanted [9]. In this case, issues such as hermeticity and biocompatibility are of paramount importance. Careful engineering design considerations at several different levels (material, device, system, test, and packaging) are critical to the success of the final product.

In this article, we first provide a tutorial overview of fabrication techniques for both hard and soft MEMS. Second, we present a few examples, developed in our laboratory, of environmentally sensitive microfluidic control systems created by integrating responsive hydrogels into MEMS structures. The last of these examples is a prototype for a microfabri-

cated, glucose-sensitive valve for closed-loop insulin delivery.

2. MEMS fabrication techniques

Most MEMS fabrication techniques have their roots in the standard manufacturing methods developed for the semiconductor industry [10–12]. Therefore, a clear understanding of these techniques is necessary for anyone starting to embark on a research and development path in the micromachining area. In addition, several MEMS-specific techniques developed for fabricating micromechanical structures have been added to the micromachinist's toolbox over the past 30 years [13–16]. In this section, we will first discuss major microfabrication techniques used most frequently in the manufacturing of microstructures. Subsequently, we will present three major "hard" MEMS technologies (bulk, surface, and high-aspect-ratio micromachining) followed by more recently introduced "soft" manufacturing methods (soft lithography and other polymer processing techniques). Although we will not be able to discuss many of these techniques in detail, numerous references are included for the readers interested in probing further.

2.1. Microfabrication techniques

Basic fabrication methods currently used in MEMS and micromachining are the same as those employed by microchip manufacturers over the last four decades. These techniques are: (1) thin-film deposition, (2) lithography, (3) etching, and (4) substrate bonding. Thin films are deposited using various chemical or physical techniques and are used for masking, isolation, and structural purposes. Subsequent to thin-film deposition, the lithography step is performed in order to transfer the designed pattern onto the substrate. This is basically identical to standard photography and printing techniques. The patterned substrate is etched using various chemicals in the liquid or gas phase. Finally, substrate bonding is used either to integrate multiple functionalities or for packaging purposes. These steps can be repeated numerous times depending on the complexity of the design and process.

2.1.1. Thin-film deposition

A wide variety of techniques are used to deposit thin films of different materials on a substrate. The selection of a suitable material for a specific application should be accompanied by determination of the appropriate deposition technique, since the properties of the deposited film will be strongly process dependent. Typical film characteristics that change with deposition technique include internal stress (tensile or compressive), conformality to the substrate topography, and adhesion to the substrate material. Occasionally, process parameters and requirements restrict the type of substrate that can be processed in a deposition system (e.g. very high temperatures or contamination concerns). The four main thin-film deposition techniques are oxidation, chemical vapor deposition (CVD), physical vapor deposition (PVD), and electrodeposition.

Oxidation is typically performed on semiconductor substrates by heating them to temperatures ranging from 800 to 1200 °C in an atmosphere containing O_2 or H_2O vapor. The result is high quality thin film of oxide (e.g. SiO_2 if the substrate is silicon).

As its name suggests, Chemical Vapor Deposition includes all deposition techniques using the reaction of chemicals in a gas phase to form the deposited thin film. The most common CVD techniques used in microfabrication are Low Pressure CVD (LPCVD) and Plasma Enhanced CVD (PECVD). These methods are typically used to deposit inorganic materials such as silicon dioxide, silicon nitride, and polycrystalline silicon (polysilicon). LPCVD is performed at pressures ranging from 0.1 to 1 Torr and temperatures in the range of 550–900 °C. The deposited material can be highly stoichiometric and the films obtained are usually very conformal to the substrate's surface. PECVD is carried out in plasma systems at much lower temperatures, which is often the reason for its choice. However, the obtained films are often less conformal and of poor quality.

Physical vapor deposition systems are based on two different principles: evaporation and sputtering. In evaporation systems, a piece of the material to be deposited is heated in a vacuum chamber containing the substrate. The evaporated material is spread all over the chamber and a thin film is deposited on top of the substrate. (As a more macroscopic example, mirrors can be formed by evaporative deposition of

silver wire onto plate glass.) In sputtering, a target of the material to be deposited is bombarded with high-energy inert ions (usually argon). The outcome of the bombardment is that individual atoms or clusters are removed from the surface and ejected towards the substrate. Due to the directionality of the arriving material, physical vapor-deposited films are nonconformal. Metals are easily deposited using these techniques, although many other materials can also be evaporated or sputtered.

Electrodeposition (or electroplating) is a process typically used to obtain thick (tens of micrometers) metal structures. In this electrochemical process, the substrate is introduced in a solution containing a reducible form of the ion of the desired metal and is maintained at a negative potential (cathode) relative to a counter electrode (anode). The ions are reduced at the sample surface and the non-soluble metal atoms are deposited.

2.1.2. Lithography

Lithography is the technique used to transfer a computer-generated pattern onto a substrate (silicon, glass, etc). This pattern is subsequently used to etch an underlying thin-film (oxide, nitride, etc.) for various purposes (doping, etching, etc.). The starting point subsequent to the creation of the computer layout for a specific fabrication sequence is the generation of a photomask. This involves a sequence of photographic processes (using optical or e-beam pattern generators) which results in a glass plate having the desired pattern in the form of a thin (~ 100 nm) chromium layer. Following the generation of photomask, the lithography process can proceed as shown in Fig. 1. After depositing the desired material on the substrate, the photolithography process starts with spin-coating of the substrate with a photosensitive resist material to a thickness of 0.5–2.5 μm, depending on viscosity and spin speed. Following spinning, the substrate is soft-baked (5–30 min at 60–100 °C) in order to remove solvents from the resist and improve adhesion. Subsequently, the mask is aligned to the wafer and the photoresist is exposed to a UV source. For most MEMS fabrications, a g-line (436 nm) mercury source is more than adequate.

After exposure, the photoresist is developed by washing off the UV-exposed or the unexposed regions, depending on whether the resist material is "positive" or "negative", respectively. (This process is similar to the development of photographic film.) The resist is subsequently hard-baked (20–30 min at 120–180 °C) in order to further improve the adhesion. The hard-bake step concludes the photolithography sequence by creating the desired pattern on the wafer. Next, the underlying thin film is etched away and photoresist is stripped in acetone or other organic removal solvents.

Although both positive and negative resist materials are available, positive resist is most extensively used in very large scaled integration (VLSI) processes, due to its superior performance with regard to the process control in small geometries.

2.1.3. Etching

As mentioned above, a lithography step is usually followed by an etching step in order to obtain a patterned film or selective material removal from the substrate. Two important figures of merit for any etching process are selectivity and directionality. Selectivity is the degree to which the etchant can differentiate between the masking material and the material to be etched. Directionality has to do with the etch profile under the mask. In an isotropic etch, the etchant attacks the material in all directions at the same rate, hence, creating a semi-circular profile under the mask, as shown in Fig. 2a. In an anisotropic etch, the dissolution rate depends on specific directions, and one can obtain straight sidewalls, as in Fig. 2b, or other non-circular profiles.

One can also divide the various etching techniques into the "wet" and "dry" categories. Wet etchants are by and large isotropic in reactivity and show superior material selectivity as compared to various dry techniques. Due to the lateral undercut, the minimum feature achievable with wet isotropic etchants is limited to >3 μm. An extremely important exception to this rule is provided by the anisotropic wet etching of monocrystalline substrates. The development of anisotropic etching of crystalline silicon is considered to have marked the beginning of micromachining and the MEMS discipline.

The three most important anisotropic silicon etchants are potassium hydroxide (KOH), ethylene diamine pyrochatechol (EDP), and tetramethyl ammonium hydroxide (TMAH). These etchants attack silicon along preferred crystallographic directions. In addition, they all show a marked reduction in the etch rate

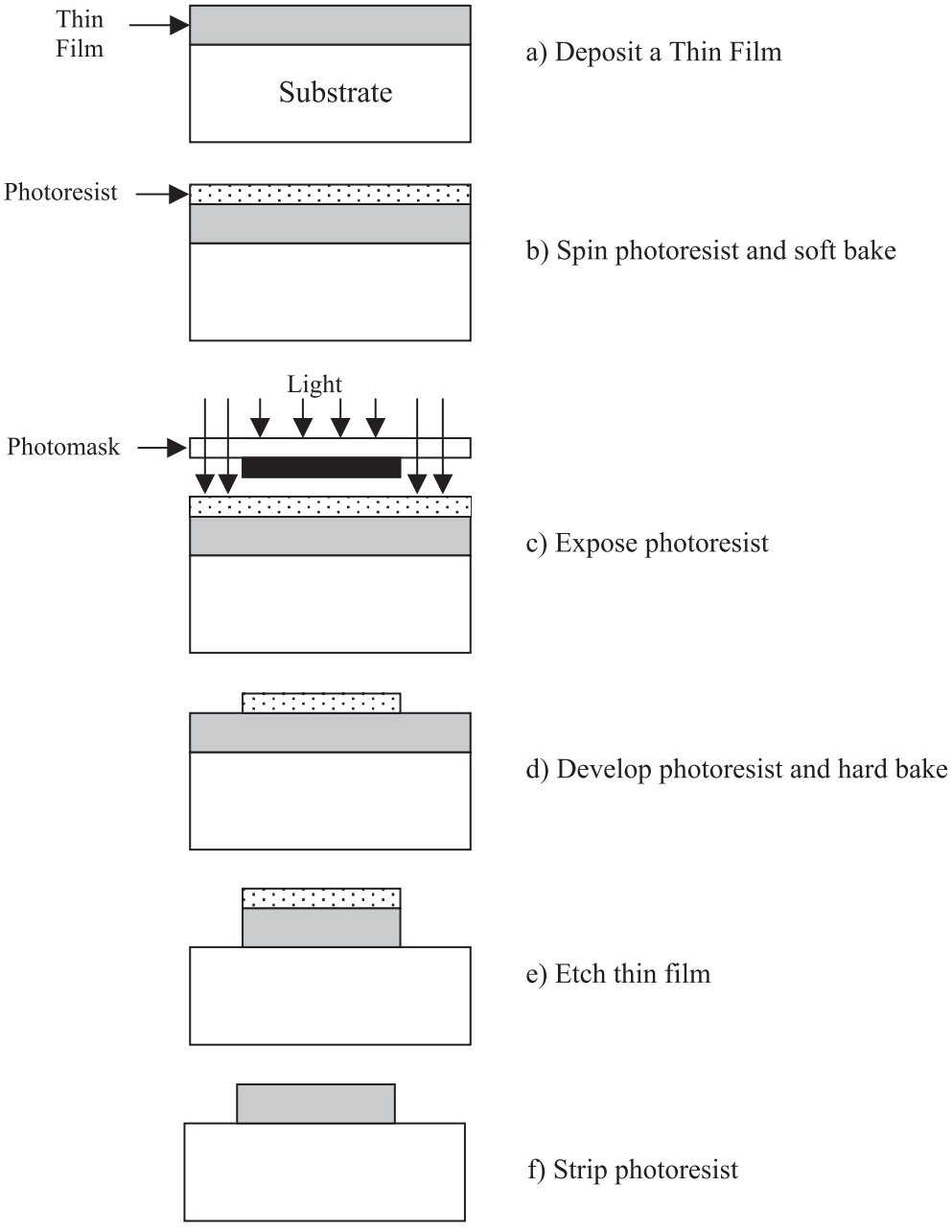

Fig. 1. Schematic drawing of the photolithographic steps with a positive photoresist. Reproduced with permission from Fig. 2 in [57] (© 2004 Springer).

in heavily doped ($>5 \times 10^{19}$ cm^{-3}) boron (p^{++}) regions. Common masking materials for anisotropic wet etchants are silicon dioxide and silicon nitride, with the latter being superior for longer etch times. The crystallographic plane showing the slowest etch rate is the <111> plane, while the fastest etch occurs into the <100> plane. The anisotropic behavior of these etchants has been used extensively to create beams, mem-

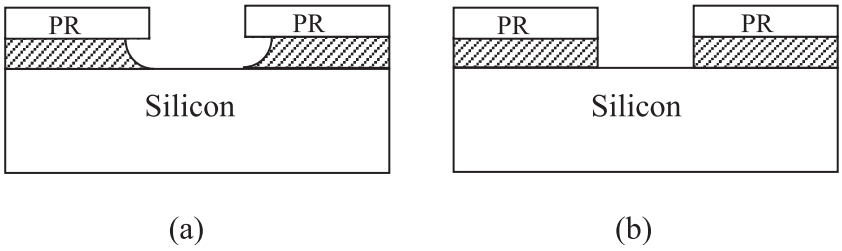

Fig. 2. Profile for (a) isotropic and (b) anisotropic etch through a photoresist mask. Reproduced with permission from Fig. 11 in [57] (© 2004 Springer).

branes, and other mechanical and structural components (see the bulk micromachining section below).

Dry etching has several advantages compared to the wet etching techniques. These include smaller undercut (allowing smaller lines to be patterned) and higher anisotropicity (allowing high aspect ratio vertical structures). However, selectivity is lower than with wet etching. The three basic dry etching techniques, namely High-Pressure Plasma Etching, Reactive Ion Etching (RIE), and Ion Milling utilize different mechanisms to obtain directionality.

Ion milling is a purely physical process, which utilizes accelerated inert ions (e.g. Ar^+) striking perpendicular to the surface to remove material (pressure $\sim 10^{-4}$–10^{-3} Torr). The main characteristics of this technique are very low etch rates (in the order of a few nm/min) and poor selectivity (close to 1:1 for most materials).

In high-pressure (0.1–5 Torr) plasma etching, highly reactive species are created that react with the material to be etched. The products of the reaction are volatile so that they diffuse away and new material is exposed to the reactive species.

RIE etching, also called "ion-assisted etching", is a combination of physical and chemical processes. In this technique, the reactive species react with the material only when the surfaces are "activated" by the collision of incident ions from the plasma (e.g. by breaking bonds at the surface). The directionality of the ions' velocities produces many more collisions with the horizontal surfaces than with the walls, thus generating faster etching rates in the vertical direction.

To further increase etch anisotropy, in some cases, sidewall passivation methods are used. An interesting case is Deep Reactive Ion Etching (DRIE) technique, often called "deep trench etching", which is capable of achieving aspect ratios of 30:1 and silicon etching rates of 2 to 3 μm/min. In this technique, illustrated in Fig. 3, an already etched pit is coated with a passivation layer of polymer, followed by ion bombardment. Ions are directed against the bottom of the pit, etching the bottom polymer and a thin layer of underlying substrate, but leaving the sidewalls intact. This process is repeated numerous times until an etched pit of desired depth results. (In fact, straight etching all the way through a wafer is possible by this method.)

In commercial silicon DRIE etchers, SF_6/Ar is typically used in the etching step and a combination of Ar^+ and a fluoropolymer (nCF_2) is used in the passivation step. A Teflon™-like polymer about 50 nm thick is deposited during the latter step, covering only the vertically oriented side-walls, since Ar^+ bombardment removes the Teflon on the bottom, horizontal surfaces.

2.1.4. Substrate bonding

Substrate (wafer) bonding (silicon–silicon, silicon–glass, and glass–glass) is one of the most important fabrication techniques in microsystem technology [17]. It is frequently used to fabricate complex 3-D structures, both as a functional unit and as a part of the final microsystem packaging and encapsulation. The two most important bonding techniques are silicon–silicon fusion (or silicon direct bonding) and silicon–glass electrostatic (or anodic) bonding. In addition to these techniques, several other alternative methods which utilize an intermediate layer (eutectic, adhesive, and glass frit) have also been investigated.

Direct silicon or fusion bonding is used in the fabrication of micromechanical devices and silicon-on-insulator (SOI) substrates. This technique is used primarily to bond two silicon wafers with or without

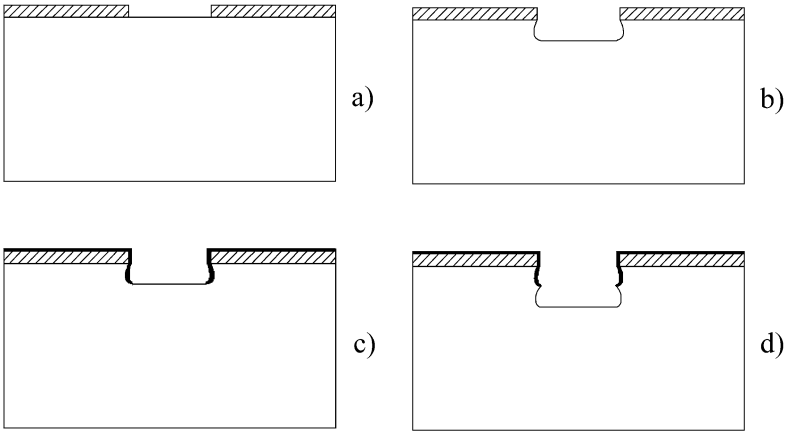

Fig. 3. Deep reactive ion etching (DRIE) process: (a) photoresist patterning, (b) etch step, (c) passivation step, (d) etch step. Steps (c) and (d) may be repeated until desired depth is achieved. Reproduced with permission from Fig. 16 in [57] (© 2004 Springer).

an oxide layer. The bonding procedure is as follows: the silicon or oxide-coated silicon wafers are first thoroughly cleaned. Subsequently, the surfaces are rendered hydrophilic by hydroxylation in HF or boiling nitric acid (RCA clean also works). The substrates are then brought together in close proximity, starting from the center to prevent void formation. As a result, attractive van der Waals forces bring the surfaces into intimate contact on an atomic scale, and hydrogen bonds form between the two hydroxylated surfaces, joining the substrates together. These steps can be performed at room temperature; however, in order to increase the bond strength, a high temperature anneal is usually required (800–1200 °C). A major advantage of silicon fusion bonding is the thermal matching of the substrates.

Silicon–glass anodic (electrostatic) bonding is another major substrate joining technique which has been extensively used for microsensor packaging and device fabrication. The main advantage of this technique is its lower bonding temperature. Fig. 4 shows a schematic diagram of the bonding setup. A glass wafer (usually Pyrex 7740 due to its thermal expansion match to silicon) is placed on top of a silicon wafer and the sandwich is heated to 300–400 °C. Subsequently, a voltage of ~1000 V is applied to the glass–silicon sandwich with the glass connected to the cathode. Bonding starts immediately upon appli-

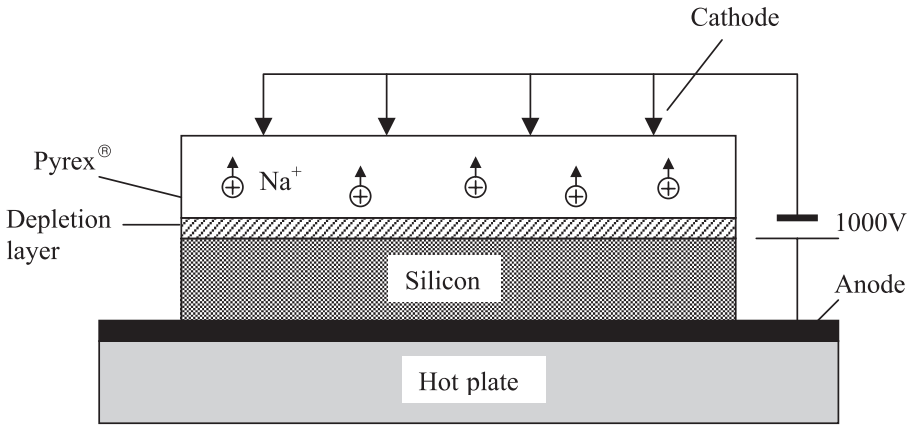

Fig. 4. Glass to silicon anodic bonding setup. Reproduced with permission from Fig. 17 in [57] (© 2004 Springer).

cation of the voltage and spreads outward from the cathode contact points. During the heating period, glass sodium ions move toward the cathode and create a depletion layer at the silicon–glass interface. A strong electrostatic force is therefore created at the interface, which pulls the substrates into intimate contact, apparently creating conditions for covalent silicon–oxygen bonds to form at the interface. The precise chemistry underlying anodic bonding has not yet been elucidated.

The techniques outlined so far are common to the semiconductor industry and to MEMS technology. We now turn to MEMS-specific methodologies.

2.2. "Hard" micromachining

2.2.1. Bulk micromachining

Bulk micromachining is the oldest MEMS technology and hence probably one of the more mature ones [18]. It is currently by far the most commercially

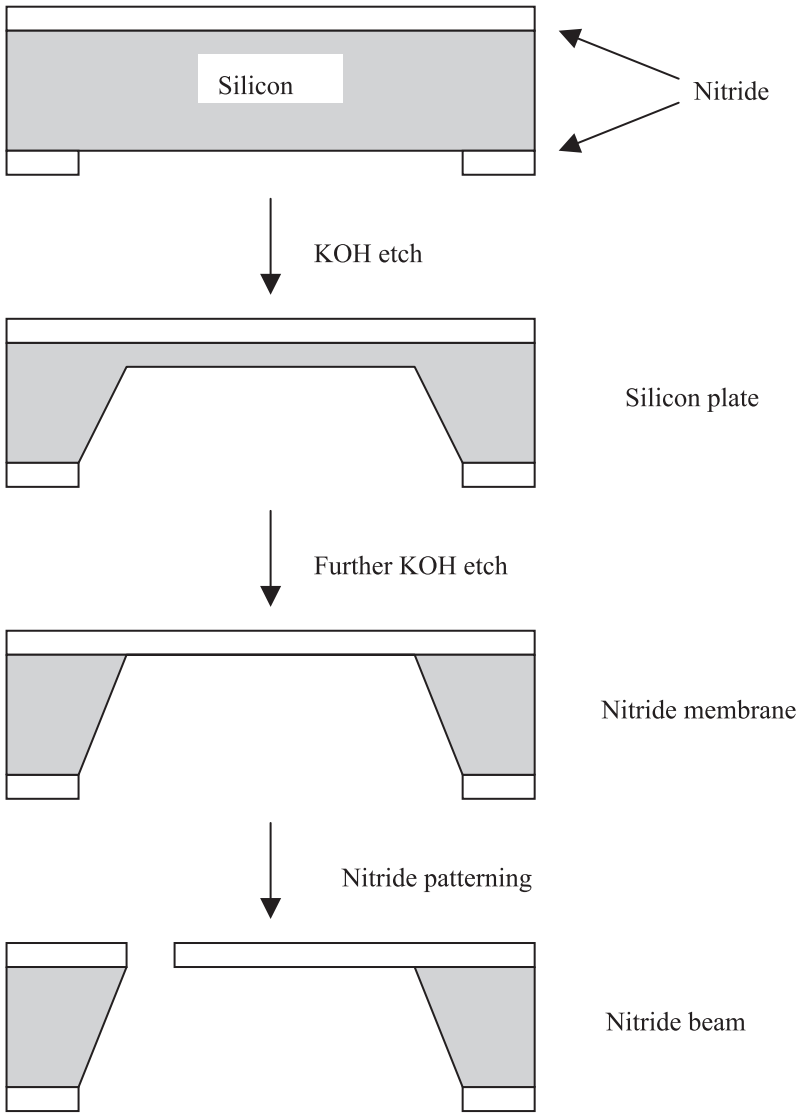

Fig. 5. Structures fabricated with bulk micromachining.

successful method used to manufacture devices such as pressure sensors and ink-jet print heads. Although there are many different variations, the basic concept behind bulk micromachining is selective removal of substrate (silicon, glass, GaAs, etc.). This allows the creation of various micromechanical components such as beams, plates, and membranes, which can be used to fabricate a variety of sensors and actuators.

The most important microfabrication techniques used in bulk micromachining are wet and dry etch and substrate bonding. The slower ⟨111⟩ plane etch rate is used to create 54.7° sloped sidewalls in a ⟨100⟩ wafer. Depending on the dimensions of the mask opening, a "V"-groove or a trapezoidal basin is formed in the ⟨100⟩ wafer. A large enough opening will allow the silicon to be etched almost all the way through the wafer, leaving a thin dielectric membrane on the other side. Back-side etching can be used to create movable structures such as beams, membranes, and plates, as shown in Fig. 5.

It is also possible to merge wet bulk micromachining and microelectronics fabrication processes to build micromechanical components on the same substrate used in integrated circuits (CMOS, Bipolar, or BiCMOS) [19]. This combination is very appealing since it allows the integration of interface and signal processing circuitry with MEMS structures on a single chip. However, important fabrication issues such as process compatibility and yield have to be carefully considered. Among the most popular techniques in this category is post-processing the CMOS integrated circuits by front-side etching in TMAH solutions. Fig. 6 shows a schematic of a process in which front-side wet etch and electrochemical etch stop have been used to produce suspended beams. This technique has been extensively used to fabricate a variety of microsensors (e.g. humidity, gas, chemical, and pressure).

Bulk silicon micromachining techniques using dry etch represent a very attractive alternative to the wet techniques described in the previous section. These techniques were developed during the mid-1990s subsequent to successful efforts geared towards the development of processes for anisotropic dry silicon etch. More recent advances in deep silicon RIE and the availability of SOI wafers with a thick top silicon layer have increased the application of these techniques. These techniques allow the fabrication of high aspect ratio vertical structures in isolation or along with on-chip electronics. Process compatibility with active microelectronics is less of a concern in dry methods since many of them do not damage the circuit or its interconnect.

The simplest dry bulk micromachining technique relies on front side undercut of microstructures using XeF_2 vapor phase etch. This however is an isotropic etch and therefore has limited application. A combination of isotropic/anisotropic dry etch is more useful and can be used to create a variety of interesting structures. For example, the Single-Crystal Reactive Etching and Metallization (SCREAM) technique relies on the combination of isotropic/anisotropic dry etch to create single crystalline suspended struc-

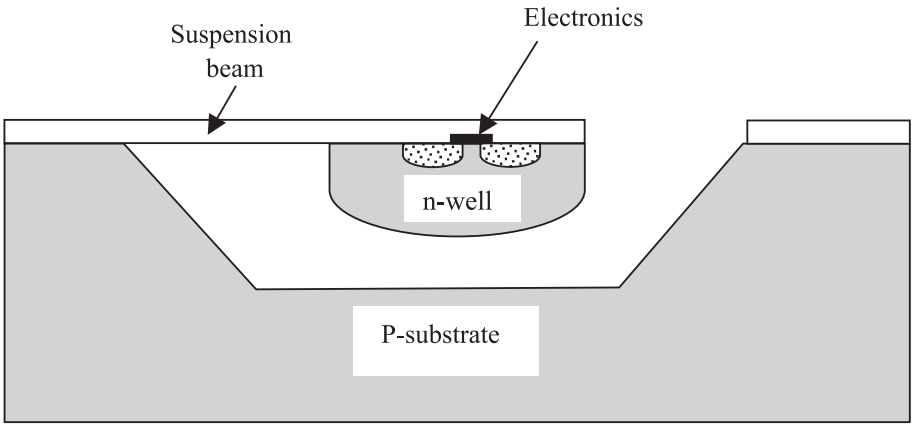

Fig. 6. Suspended island created on a prefabricated CMOS chip using front-side wet etch and electrochemical etch stop. Reproduced with permission from Fig. 25 in [57] (© 2004 Springer).

tures [20]. Fig. 7 shows the cross-section of the process. It starts with an anisotropic (Cl_2/BCl_3) silicon etch using an oxide mask (Fig. 7a–b). This is followed by a conformal PECVD oxide deposition (Fig. 7c). Subsequently, an anisotropic oxide etch is used to remove the oxide at the bottom of the trenches leaving the sidewall oxide intact (Fig. 7d). At this stage, an isotropic silicon etch (SF_6) is performed which results in undercut and finalization of the silicon structures (Fig. 7e). Finally, if electrostatic actuation is desired, a metal can be sputtered to cover the top and sidewall of the microstructure and bottom of the cavity formed below it (Fig. 7f).

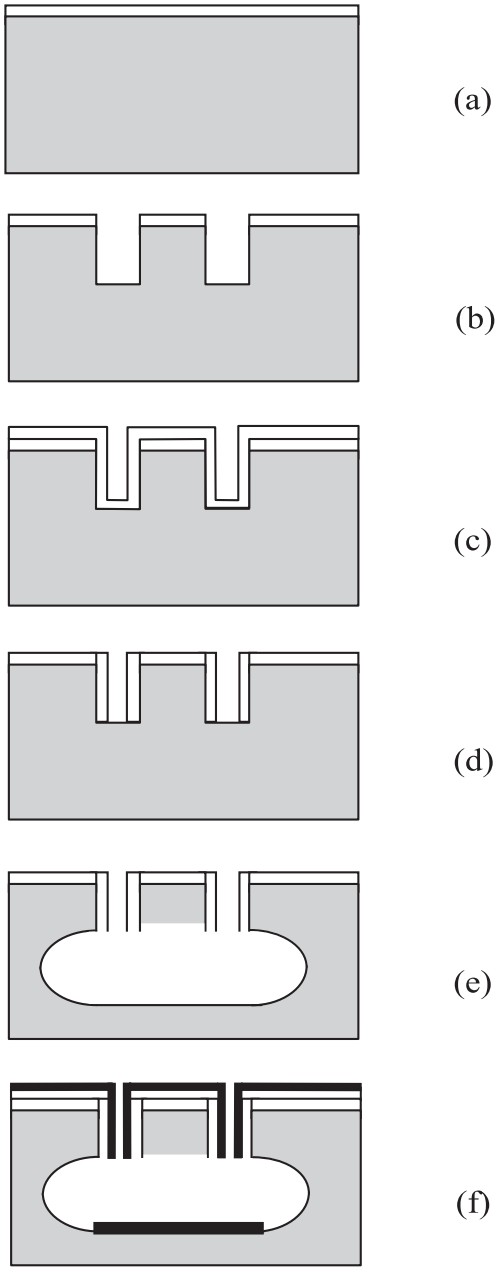

Fig. 7. Cross-section of the SCREAM process. See text for description of steps. Reproduced with permission from Fig. 27 in [57] (© 2004 Springer).

2.2.2. Surface micromachining

Surface micromachining is another important MEMS microfabrication technique that can be used to create movable microstructures on top of a silicon substrate [21]. This technique relies on the deposition of structural thin films on a sacrificial layer which is subsequently etched away resulting in movable micromechanical structures (beams, membranes, plate, etc.). The main advantage of surface micromachining is that extremely small sizes can be obtained. In addition, it is relatively easy to integrate the micromachined structures with on-chip electronics for increased functionality. However, due to the increased surface nonplanarity with any additional layer, there is a limit to the number of layers that can be deposited.

The basic surface micromachining process is illustrated in Fig. 8. The process begins with a silicon substrate on top of which a sacrificial layer is grown and patterned (Fig. 8a). Subsequently, the structural material is deposited and patterned (Fig. 8b). As can be seen, the structural material is anchored to the substrate through the openings created in the sacrificial layer during the previous step. Finally, the sacrificial layer is removed, leaving behind the desired microstructures (Fig. 8c).

In wide structures, it is usually necessary to provide access holes in the structural layer for fast sacrificial layer removal. The most common sacrificial and structural materials are phosphosilicate glass (PSG) and polysilicon, respectively (low temperature oxide or LTO is also frequently used as the sacrificial layer). However, there are several other sacrificial/structural combinations that have been used to create a variety of surface micromachined structures. Two commercially available examples surface illustrate successful sacrificial/structural combinations. First, the Texas Instruments (TI) deformable mirror

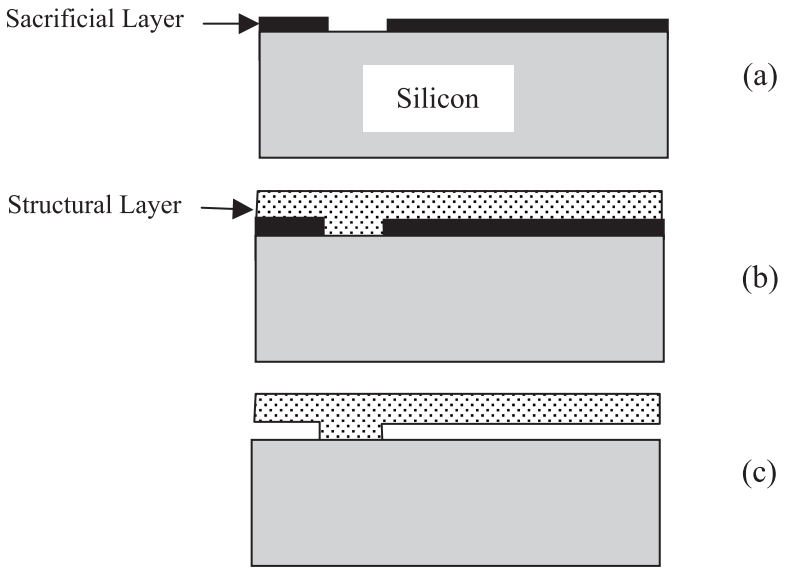

Fig. 8. Basic surface micromachining fabrication process. See text for description of steps. Reproduced with permission from Fig. 32 in [57] (© 2004 Springer).

display (DMD) [22] spatial light modulator uses aluminum as the structural material (good optical reflectivity) and photoresist as the sacrificial layer (easy dry etch and low processing temperatures, allowing easy post-IC integration with CMOS). Second, the Analog Devices microgyroscope uses polysilicon structural material and a PSG sacrificial layer [23].

An important consideration in the design and processing of surface micromachined structures is the issue of stiction [21], which can occur either during fabrication when a wet etchant is used to remove the sacrificial layer, or during the device lifetime. The source of stiction during fabrication is surface tension of the liquid etchant, which can pin the microstructure down. This usually occurs when the structure is compliant and does not possess a large enough spring constant to overcome the surface tension force of the rinsing liquid (i.e., water). There are several ways to alleviate stiction during fabrication, including: (1) the use of dry or vapor phase etchant; (2) the use of solvents with lower surface tension, such as methanol; (3) geometrical modifications, e.g. introduction of dimples between the formed structures; (4) CO_2 critical drying; (5) freeze drying; and (6) self-assembled monolayer (SAM) or organic thin-film surface modification.

Stiction that occurs during the operating lifetime of the device (in-use stiction) is due to the condensation of moisture on the surfaces, electrostatic charge accumulation, or direct chemical bonding. Surface passivation using self-assembled monolayers or organic thin films can reduce the surface energy, reduce or eliminate capillary forces, and direct chemical bonding. Direct application of organic thin layers to the semiconductor (absent an intervening oxide layer) also reduces electrostatic forces.

2.2.3. High-aspect-ratio micromachining

High-aspect-ratio micromachining is an important addition to the MEMS-based manufacturing techniques that can be used to fabricate a variety of biomedical microdevices which would be difficult to make using the more or less inherently 2-D bulk and surface technologies. The most common high-aspect-ratio technology is LIGA (in German: Lithographie Galvanoformung Abformung) [24]. The three basic fabrication steps illustrated in Fig. 9 are: (a) X-ray lithography over a thick resist layer, (b) electroplating to fill the exposed and developed areas with a metal, and (c) removal of the resist. The metal structures have vertical sidewalls and have thicknesses in the range of a few microns to a few

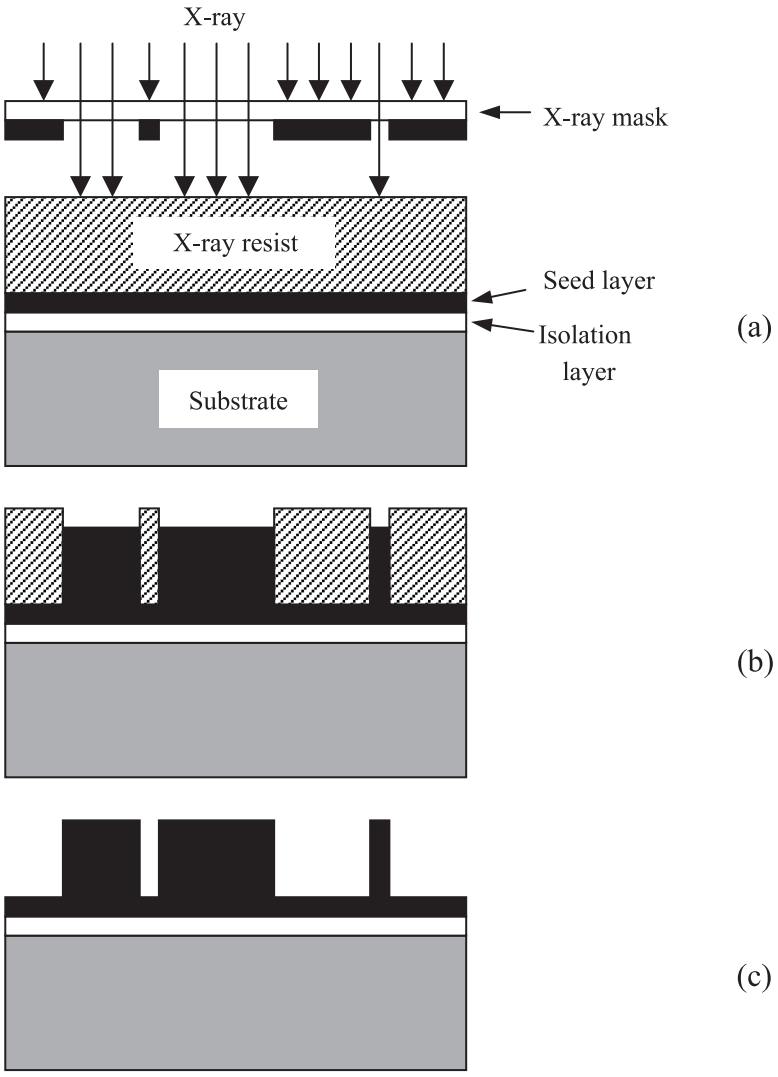

Fig. 9. Cross-section of LIGA process: (a) X-ray exposure of resist, (b) resist development and electroplating, and (c) strip the resist.

millimeters. This is achieved using high-energy (synchrotron) X-ray lithography and special photoresists. Due to their short wavelengths, high-energy X-rays are capable of penetrating a thick photoresist layer without scattering. This results in high-aspect-ratio features with lateral dimensions down to 0.2 μm (aspect ratio >100:1). These metallic structures can be used as a mold in order to fabricate plastic injection molded parts. The photoresists used in LIGA should comply with certain requirements, including sensitivity to X-rays, resistance to electroplating chemicals, and good adhesion to the substrate. Based on such requirements, poly(methylmethacrylate) (PMMA) is considered to be the optimal choice.

High cost and limited access to synchrotron X-ray machines have prevented the widespread use of the LIGA processes. This has resulted in the development of an inexpensive alternative called the UV-LIGA or "poor man's LIGA" [25,26]. This process uses SU-8 negative photoresists (available for spin coating at various thickness ranging from 1 to 500 μm) and standard contact lithography equipment. Using this

technique, aspect ratios larger than 20:1 have been demonstrated.

2.3. "Soft" micromachining

As was mentioned previously, in the biomedical MEMS area, soft materials (polymers and gels) have some unique advantages over silicon and glass. The fabrication of micropatterns and microstructures with soft materials, sometimes called "soft lithography", is based on two old techniques: molding and embossing. Polydimethylsiloxane (PDMS), also known as silicone rubber, is the material of choice for micromolding. PDMS is inexpensive, biocompatible, and has excellent sealing properties, making it very suitable for microfluidics [27]. In addition, it can be easily bonded to itself, allowing the fabrication of multilayer structures. Finally, thin PDMS diaphragms are elastically extensible so that much larger deflections can be achieved than with hard materials.

Fabrication of PDMS structures with micromolding is illustrated in Fig. 10. First, a mold is fabricated using any of the previously discussed hard micromachining techniques. Depending on the mold material and topography, a surface treatment is usually recommended in order to facilitate demolding. Subsequent to the micromold fabrication, a prepolymer solution (usually a mixture of PDMS linear polymer and a crosslinking agent) is poured on top of the mold. For high-aspect-ratio mold topographies, this step may need to be performed under vacuum to remove air bubbles. Once polymerization is completed (1–24 h depending on the curing temperature), the PDMS layer is carefully peeled off. The mold can be reused many times, which reduces the cost considerably. Multilayer soft lithography that combines soft lithography with the capability to bond multiple patterned layers of PDMS has also been used to fabricate monolithic blocks of PDMS with various levels of microchannels [28]. One can also insert a thin PDMS diaphragm in between two microchannels containing layers forming pneumatically actuated valves and peristaltic pumps by applying a positive pressure to the top channel. This results in the deflection of the membrane and blocking of fluid passage in the bottom channel. Extensibility of the PDMS diaphragm is controlled by its thickness, aspect ratio, and the amount of crosslinker in the prepolymer. PDMS bonds well to itself, glass, and silicon nitride. Bonding of PDMS to other materials is facilitated by surface pretreatment with plasma or HCl.

Hot embossing of plastics such us polycarbonate and PMMA has also been explored as an inexpensive alternative to microfabrication with silicon and glass [29]. For example, quartz templates having the negative image of microchannels have been used to produce a PMMA microfluidic chip for DNA separation and detection [30]. Fig. 11 shows the process schematic. First the stamp or master is brought in contact with the plastic surface. A uniform distributed

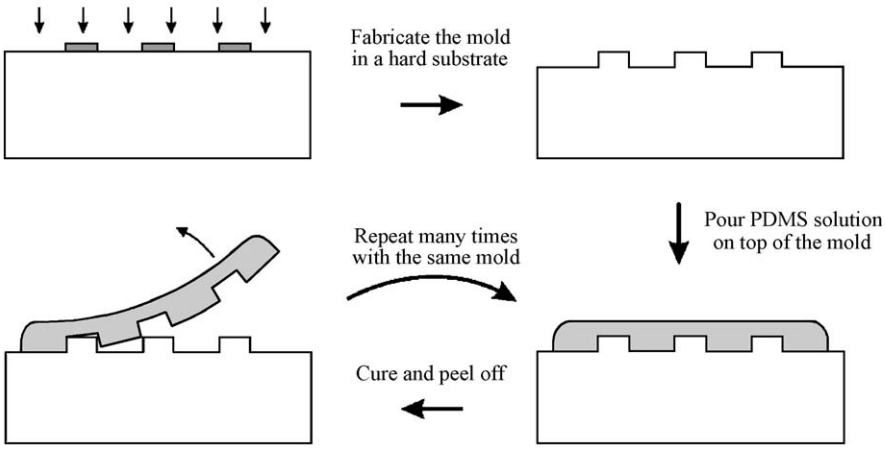

Fig. 10. Micromolding process.

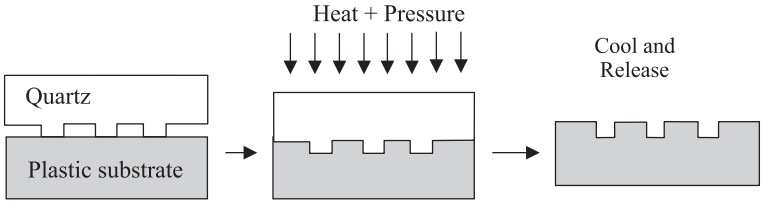

Fig. 11. Hot embossing process. See text for description of steps.

pressure is then applied while the substrate is heated to above its glass transition temperature. Finally, the substrate is cooled down before removing the stamp. Hot embossing has also proved to be an effective technique for nanoscale fabrication and has found many applications in the optical technologies. Microlenses, diffraction grating, and optical waveguides are some examples of optical components fabricated by this technique [31].

Recently, a set of techniques for micromachining of polymeric materials called "microfluidic tectonics" (μFT) was introduced by Beebe et al. [32]. Briefly, this approach, which is particularly useful for rapid prototyping of MEMS constructs, is based on photopolymerization under a series of masks whose purpose is to prevent polymerization in specific regions. After a photopolymerization step is completed, unreacted monomer can be flushed, with retention of the polymerized features, which may be hard or soft depending on whether the polymer is glassy or rubbery, respectively. Multiple features can be produced either in parallel (during polymerization under a single mask), or in series (as a result of a sequence of photopolymerizations under different masks.) Because they polymerize rapidly and with minimal change in volume, the monomers isobornyl acrylate and tetraethylene glycol dimethacrylate (crosslinker) constitute an excellent pair, which can be polymerized into hard structures under UV irradiation in the presence of the photoinitiator Irgacure 651. Soft structures such as hydrogels can also be photopolymerized under mask.

As a simple example, a mask consisting of a straight line, placed over the prepolymer solution, will lead to a microfluidic channel after UV exposure and flushing. An aqueous prehydrogel solution can then be introduced into the channel, and then photopolymerized under a grating that periodically (in space) passes and blocks UV light. After flushing, the result will be a channel in which empty space is periodically interrupted by hydrogel. More elaborate hydrogel-μFT devices are described by Eddington and Beebe in this issue [33].

Microfluidic tectonics possesses many advantages with regard to flexibility and ease of processing. There are, however, limitations in the size of and packing density of structures, which arise from diffraction, reflection, and scattering of the incident UV light and the existence of a "penumbra" of polymerization around the directly irradiated region. Thus, μFT features below 50 μm tend to be difficult to fabricate. This limit can be addressed, however, by trading off device depth for increased lateral resolution, or by moving to more expensive multiphoton sources that permit resolution on the submicron scale.

An additional limitation in the use of soft stimuli-sensitive materials, such as hydrogels, lies in the geometric reproducibility of the resultant structures. Because the structures swell upon exposure to different chemical environments after polymerization, their final shape depends on a broader set of factors compared to those encountered with solid phase lithography.

To date, μFT has proven most useful for rapid prototyping, but the flexibility in the choice of materials and ease of integration with other processes make μFT an intriguing platform for future exploration.

3. Examples of microfabrication using stimuli-responsive hydrogels

As already indicated in our discussion of μFT, hydrogels can be incorporated into microfluidic devices. When the swelling of such hydrogels is environmentally sensitive, the latter can be utilized to regulate flow. In this section, a set of MEMS devices

in which hydrogels are incorporated for fluid flow control is described. The last of these devices is a prototype for a microfluidic, glucose-sensitive insulin delivery device.

3.1. Crosscut system for out-of-plane fluid flow control [34]

A simple means for incorporating hydrogels into MEMS is illustrated in Fig. 12. A 500-μm-thick presilanized pyrex wafer is scored, using a dicing saw, with several sets of four parallel trenches of thickness 120 μm, depth 300 μm, and inter-trench spacing 180 μm. The wafer is then flipped over and scored with similar sets of trenches, oriented perpendicular to the first sets. The result is a criss-cross array of trenches, with 120 × 120 × 500-μm holes passing completely through the wafer at the cross-points. This structure is placed between two glass slides, and an aqueous pregel solution is introduced by capillary action into the trenches. (Seepage of this solution into spaces between the wafer and the slides is precluded by the silanized, hydrophobic surface of the wafer.) Polymerization is then initiated thermally or by UV irradiation. The result, following removal of the sandwiching glass slides, is a hydrogel that is geometrically and permanently interlocked with the pyrex structure.

As an example, a thermosensitive, lower critical solution temperature (LCST) hydrogel consisting of poly(*N*-isopropyl acrylamide) [p(NIPA)], crosslinked with *N*,*N*'-methylenebisacrylamide [35,36] is formed in a crosscut device. Silicone tubing with ID/OD 2.0/2.5 mm is glued to both faces of the wafer, such that the 16 cross-points are contained within the aperture. Water is gravity-fed into the tubing on one side of the device, and the tubing on the other side constitutes a waste stream. Tubing is immersed alternately in "cold" (25 °C) and "hot" (40 °C) water baths. The tubing is very conductive to heat, so intralumenal water temperature equilibrates rapidly with the bath. As shown in Fig. 13, hot water flows through the system, but cold water does not. The system therefore constitutes a thermosensitive fluid flow controller.

Since the LCST for the p(NIPA) hydrogel is 33–34 °C, the hydrogel is swollen and completely fills the trenches and cross-points in cold water, as illustrated in the transmission photomicrograph of Fig. 14a. As hydrogels generally present a strong resistance to water flow, this explains the lack of flow of cold water through the system. In hot water, however, the hydrogel is inclined to collapse. Note however that interlock with the wafer prevents free deswelling. Instead, the hydrogel pulls away from the trench walls and exerts tension on the hydrogel in the cross-points, as seen in Fig. 14b. The result is an opening of the

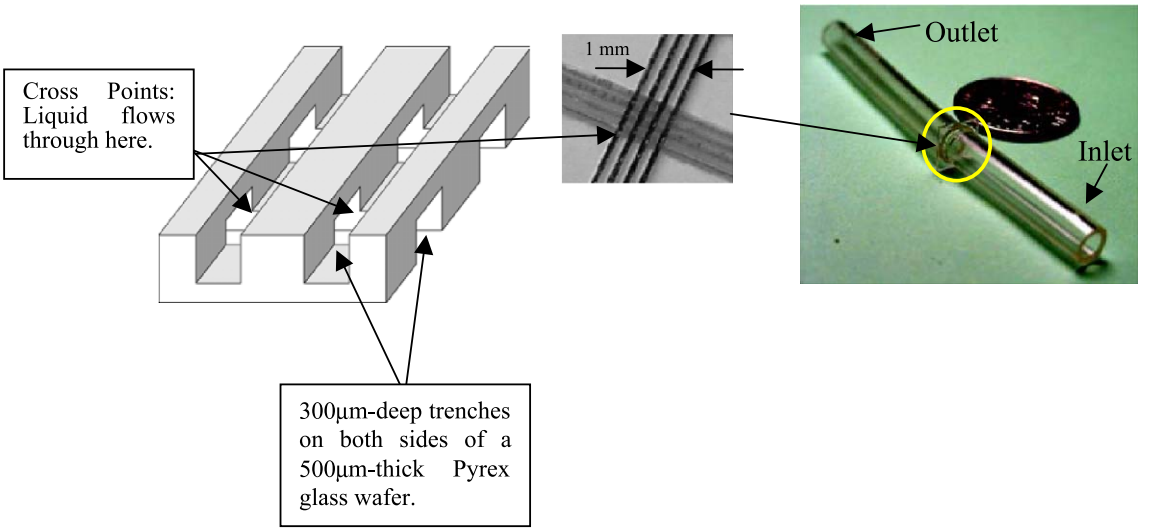

Fig. 12. Schematic of crosscut microvalve (left), photomicrograph of microvalve (center), and microvalve mounted in tubing for testing (right).

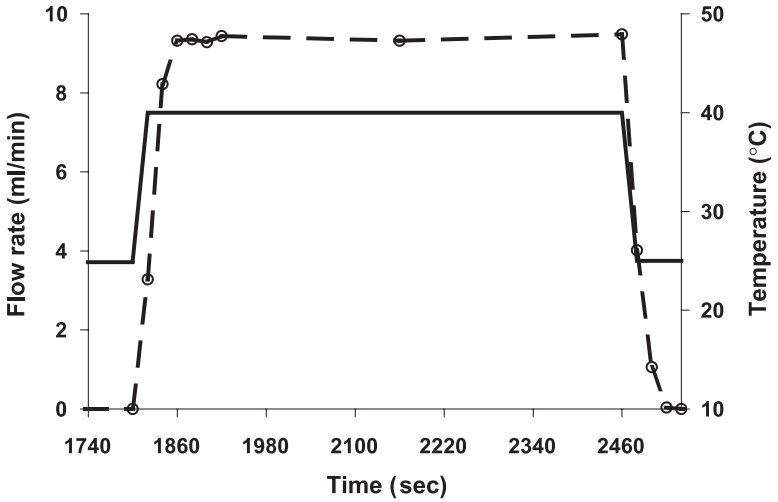

Fig. 13. Response of the flow rate (dashed line) through a temperature-sensitive poly(*n*-isopropylacrylamide) hydrogel-loaded crosscut configuration to temperature change (solid line).

cross-points at corners, providing a pathway for water flow in warm water. Note that hydrogel does not pull away from all trench walls or form holes at all corners, probably due to a mechanical instability, which prevents symmetric shrinkage. Also, the dark color of the gel in the collapsed state is due to phase separation, which occurs in p(NIPA) hydrogels upon raising of temperature. (This phase separation, which blocks

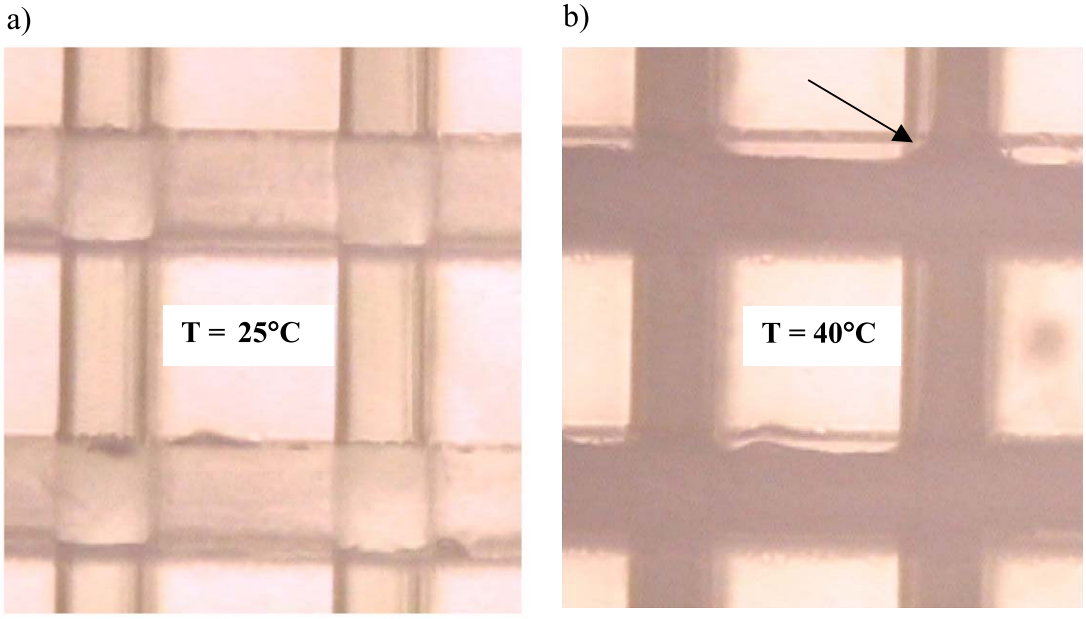

Fig. 14. (a) poly(NIPA) hydrogel completely fills trenches and cross-points in cold (25 °C) water. (b) In hot (40 °C) water, hydrogel contracts away from trench walls, exerts tension at cross-points, and opens up corners in cross-points through which water can flow (arrow). Hydrogel in hot water blocks transmission of light due to phase-separation.

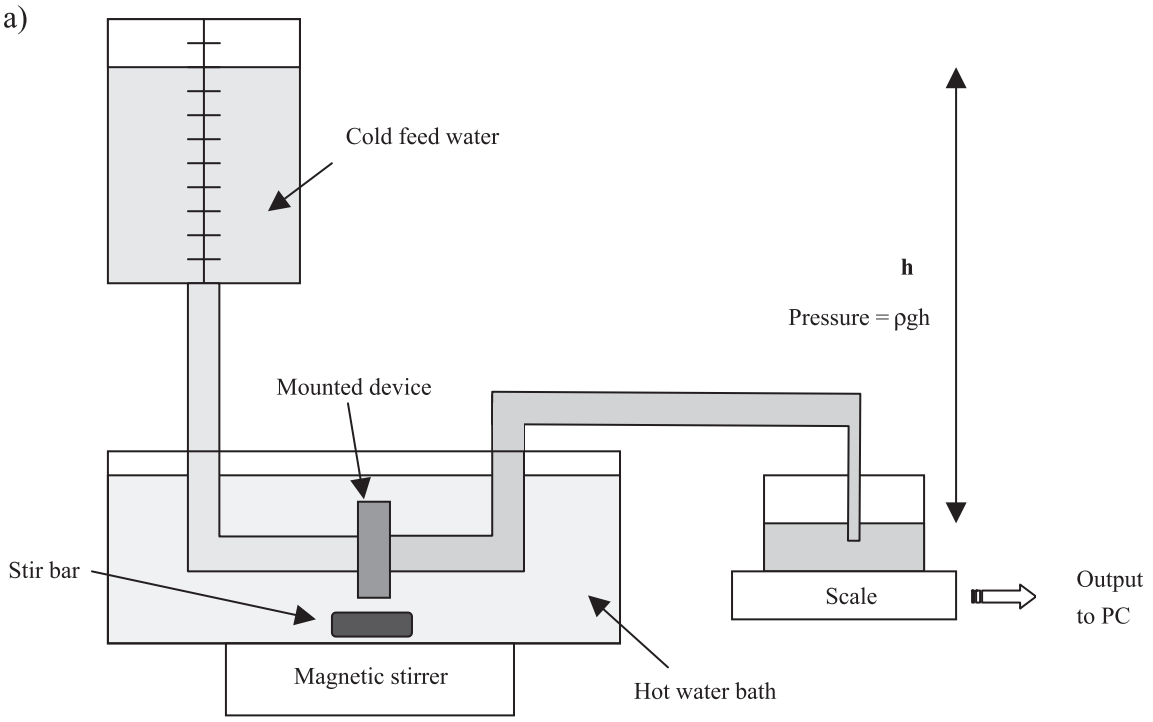

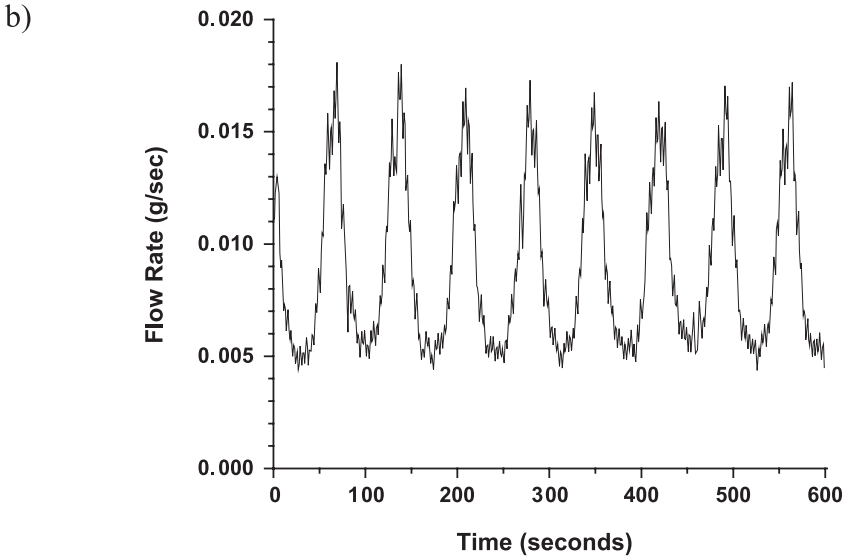

Fig. 15. (a) Schematic of thermofluidic oscillator. See text for description. (b) Thermofluidic oscillations recorded with this system.

transmission of light, may also lead to some water flow through the hydrogel.)

The response time of the thermosensitive fluid controller is seen to be about 20 s, as can be gleaned from Fig. 13. Devices containing hydrogels designed to respond to pH and other chemical stimuli may respond more slowly, since they rely on chemical diffusion, which tends to be slower than heat transfer.

The thermosensitive fluid controller just described has been incorporated into a simple thermofluidic oscillator, which switches fluid flow on and off with a regular period. In this system, illustrated in Fig. 15a, the controller is immersed in a constant temperature, hot water bath, and cold water, also at constant temperature, is gravity-fed into the lumen. When cold water is first introduced, the hydrogel swells in the trenches and shuts off fluid flow. The intralumenal water then warms up by heat conduction through the tubing, until its temperature exceeds the transition hydrogel's LCST. At this point, the hydrogel shrinks away from the trenches, opens fluid paths in the corners of the holes in the device, and water now flows through the controller. Water flows sufficiently fast that as the warmed-up water flows into the waste stream, it is replaced by cold water. Eventually, the cold water causes the hydrogel to reswell in the trenches, and water flow is shut off again, thus restarting the cycle. An example of such an oscillation is shown in Fig. 15b.

Factors affecting the period of oscillation and the fraction of time spent in the "on" and "off" state include fluid pressure, length of tubing on the "inflow" side, thermal conductivity of the tubing, temperatures of the feed and bath waters, and physicochemical characteristics of the hydrogel.

The crosscut, interlocked design just described provides a simple means to permanently fix a hydrogel in a solid substrate. In producing this system, none of the MEMS processing techniques described in previous sections was used—instead we used a simple scoring technique; consequently, feature sizes were limited to the 100-μm range. It should be clear however that wet or dry etching techniques could be used to produce much narrower channels in thinner planes. Such an approach has not been pursued yet. Instead, an alternative means of introducing hydrogels into micromachined structures to provide out-of-plane flow control, which uses an array of MEMS techniques, has been studied. This is the topic of the next section.

3.2. Tethered microvalve for out-of-plane fluid flow control [37]

In a second design, illustrated in Fig. 16, a responsive hydrogel is polymerized into an array of cylindrical orifices. Each orifice spans the thickness of a 100-μm-thick membrane formed by chemical aniso-

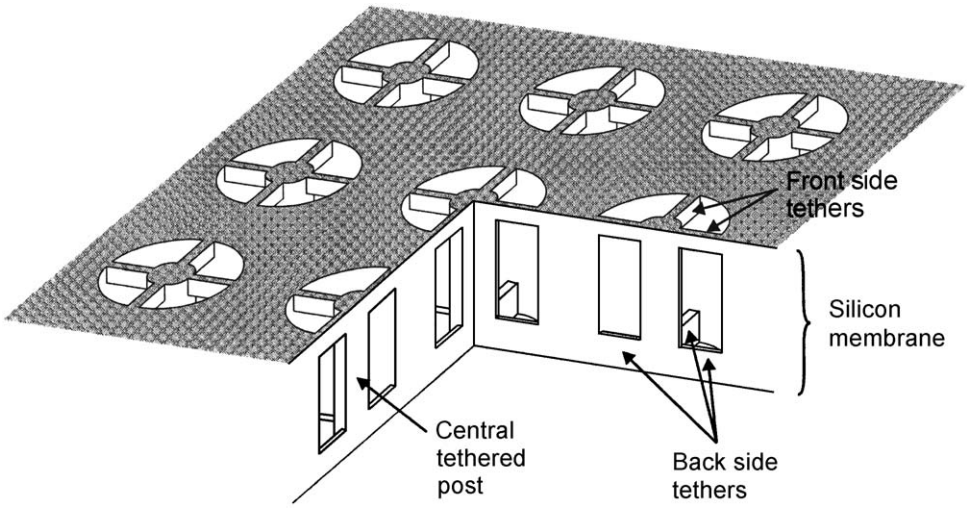

Fig. 16. Schematic of array of tethered valves microfabricated into a silicon membrane.

tropic etching of a silicon wafer, and contains a central post that is held fast by a set of tethers connecting it to the outer orifice wall at each face of the membrane. Hydrogel fills the space between the post and the outer wall, and is geometrically confined to this space. The small dimension of this hydrogel-confining structure permits a short response time.

Fig. 17 shows the basic steps of the fabrication process for the tethered structures. Fabrication starts with a 2-μm LPCVD low stress nitride deposition on standard ⟨100⟩ silicon wafers. The backside nitride is patterned and silicon is etched 400 μm in KOH, leaving a 100-μm-thick membrane sitting on top of a trapezoidal basin. Next, the front side nitride sitting atop the membrane is patterned with the wheel-like feature shown in Fig. 17c, and the non-patterned regions of silicon are deep trench etched to a depth of 80 μm, with a 20-μm layer remaining at the bottom. During this step, the central circle in the pattern defines a post, whereas the four radial projections define thin silicon spokes. Subsequently, a short KOH etch undercuts the thin spokes into triangular shape tethers. Finally, a second deep trench etch opens the orifices to the other side of the membrane and defines a second set of tethers.

Fig. 17 is a 2-D representation of a process leading to a 3-D structure, and it is not possible to show all details. Some experience is needed to visualize the actual geometries. For example, the linear "gap" in the nitride layer displayed on the bottom of the wafer in Fig. 17a is actually a rectangular, nitride-free region. Similarly, the 2-D trapezoidal etch shown in Fig. 17b represents a tapered, 3-D basin with trapezoidal sidewalls. The structures surrounded by the dashed ellipse in Fig. 17c are formed under the mask illustrated in that panel, which is placed over the front face of the membrane. Some of these features are oriented in directions that cannot be visualized straight on. Details of the process as it forms holes that cross all the way through the membrane, spokes that ultimately become tethers, and the central post, are illustrated by drawing, respectively, cross-sectional lines A–A′, B–B′, and C–C′ on the mask shown in Fig. 17c, and then following the first deep trench etch (Fig. 17d), the KOH etch (Fig. 17e), and the second deep trench etch (Fig. 17f) steps along these cross-sections, in the left, center, and right columns of those figures, respectively.

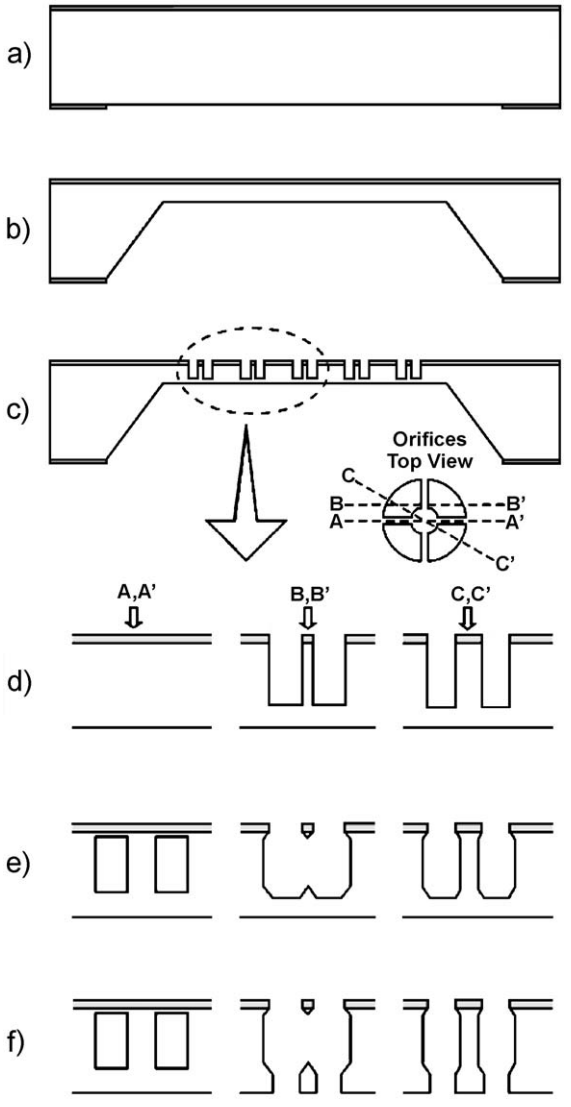

Fig. 17. Tether valve fabrication process. (a) LPCVD nitride deposition and patterning, (b) KOH etching, (c) and (d) nitride patterning and deep trench etch, (e) short KOH, and (f) deep trench etch. The three "parallel tracks" shown in (d–f) represent cross-sectional cuts along planes defined in the mask shown in (c), running through spokes (A,A′: left panels), perpendicular to spokes (B,B′: middle panels), and through the central post (C,C′: right panels).

Other aspects of Figs. 17e,f are noteworthy. First, notice that the spoke-to-tether process (B–B′, second column) leads to features that appear to be floating. These represent tethers that extend from the central post to the outer wall of the pit that is formed as a

result of the whole process. Second, the angled features are due to the same chemical etch anisotropy that leads to the tapered basin of Fig. 17b. The deep trench steps lead to straight features, however. Finally, notice that the chemical etch also attacks both the outer wall and the central post. Because these features are much thicker than the spokes, however, they are not completely undercut.

A SEM picture of the tethered valve is shown in Fig. 18. The faceted character of the central post is attributed to the differences in etch rate of KOH as it attacks different crystal planes corresponding to different angular positions around the post.

Loading of the hydrogel is achieved by immersing the devices in a small amount of pre-gel solution, followed by polymerization. Excess hydrogel is then peeled off from both sides of the membrane.

Optical micrographs of an orifice loaded with an p(NIPA) hydrogel in the swollen (low temperature) and shrunken (high temperature) states are shown in Fig. 19a,b, respectively. In the swollen state (low temperature), the hydrogel is transparent. The outer space between the shrunken hydrogel and the orifice wall is a path for fluid flow. Notice that this design provides more efficient generation of fluid flow path than does the cross-cut design.

Fig. 20 shows the response of a tethered microvalve loaded with the p(NIPA) hydrogel to changes in temperature between 25 and 50 °C. The response time is about 10 s for opening and 20 s for closing. Again, it should be recognized that chemically sensitive gating of fluid flow will be slower.

3.3. Glucose-sensitive microvalve for closed-loop insulin delivery [38]

Attempts to develop glucose-sensitive, hydrogel-based systems date back at least two decades. Early devices combined glucose oxidase (GluOx) with pH-sensitive hydrogels [39–41]. By converting glucose into gluconic acid, which readily dissociates into gluconate ion and hydrogen ion, GluOx would lower pH in the hydrogel and alter its swelling. More recently, hydrogels based on phenylboronic acid derivatives have been shown to complex directly with glucose and become charged, again altering degree of swelling [42,43]. In both cases, swelling changes are reversible. Swelling changes are ultimately converted into permeability changes to insulin [40], or are used to drive pumps [44]. Strategies in which glucose reversibly breaks crosslinks and increases gel permeability have also been pursued [45,46].

Despite advances in understanding the physicochemical nature of these swelling and permeability changes [47–51], and the elaboration of novel hydrogel chemistries to optimize response [41], there has

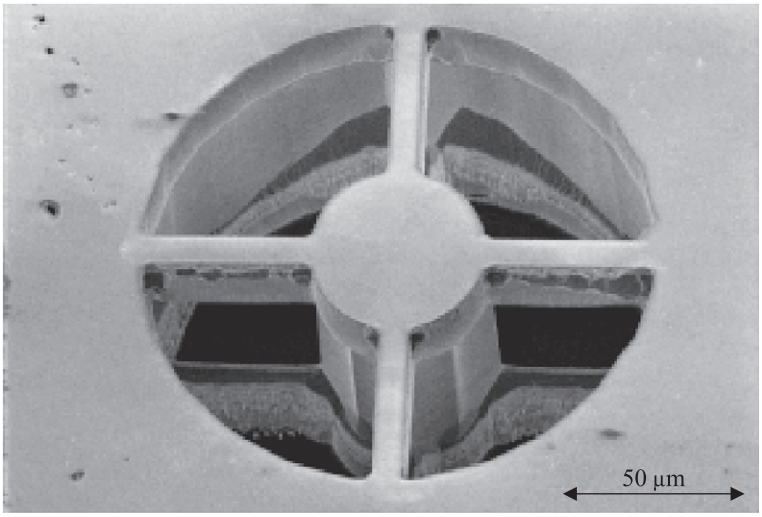

Fig. 18. Scanning electron micrograph of the silicon tethered microvalve without the hydrogel.

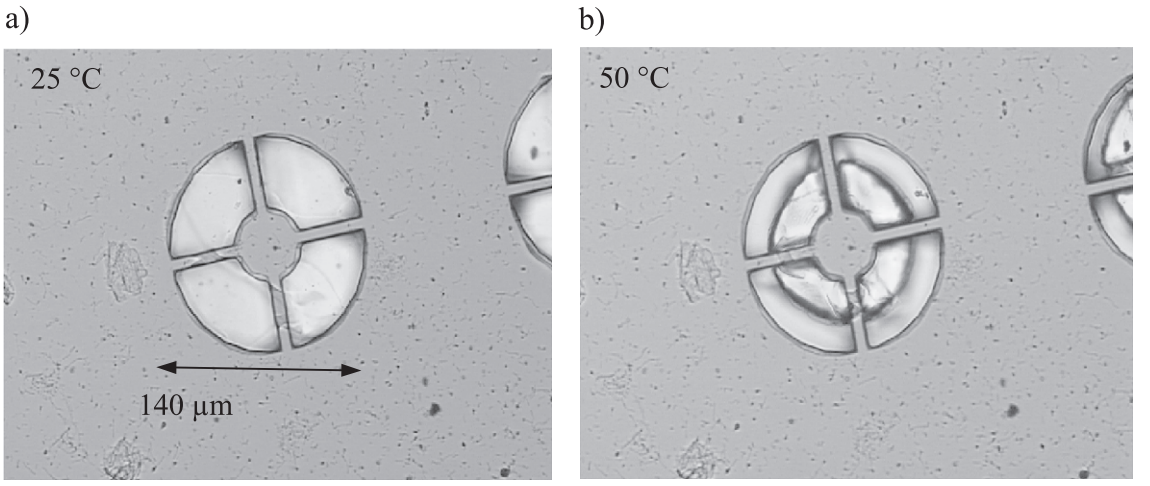

Fig. 19. Optical micrograph of hydrogel-loaded tethered microvalve in (a) the swollen, low temperature (25 °C) state, and (b) in the shrunken, high temperature (50 °C) state. Notice that valve in center is actually part of an array of identical valves.

been little success in utilizing responsive hydrogel-based systems to produce viable closed loop insulin delivery systems. We believe that several factors have contributed to this lack of success. First, hydrogels are inherently weak materials, and implanting them by themselves is not likely to lead to a physically stable delivery system. Second, while insulin is reasonably potent, the amount required (~ 1 g/year) is enough that long-term storage inside a hydrogel is not practical, even if problems surrounding protein stability inside the hydrogel could be solved. Third, there is a tradeoff between thickness of hydrogel, where an increase leads to better physical integrity and storage capacity, and the need for a short response time. Indeed, typical hydrogel-based systems require hours to develop a full response, and this is not acceptable for diabetes treatment. Fourth, none of the hydrogels thus far studied are known to be biocompatible over

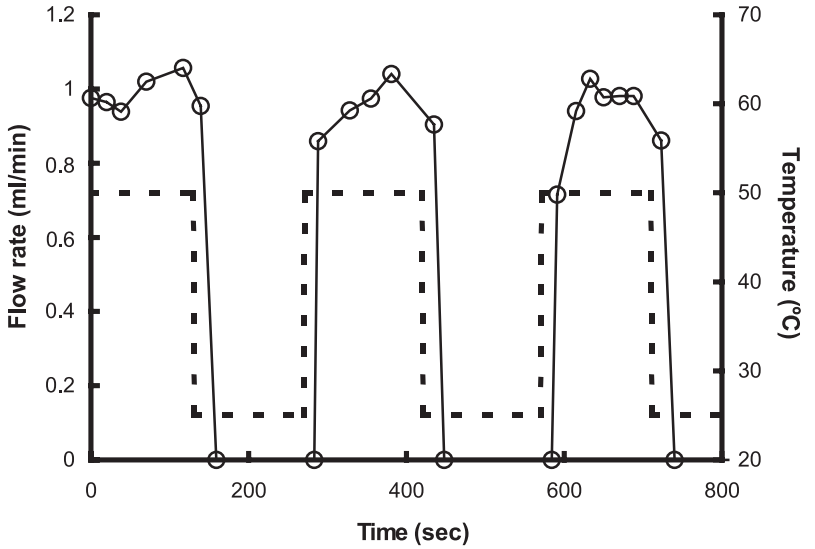

Fig. 20. Flow rate through tethered valve (open circle) vs. time when alternating temperature between 25 and 50 °C (dashed line).

long durations, and special surface modification will probably be needed to prevent protein fouling and tissue response.

Because insulin is so potent, and because overdose leads to coma and death, extra care must be exercised in its packaging. While in the future, it may be possible to implant a long-term supply of insulin, safety must be absolutely guaranteed, and it may be a long time before regulatory and consumer confidence will permit this.

With these considerations in mind, we have been developing a glucose-sensitive microfluidic valve. Such a valve would be placed at the tip of a catheter passing transcutaneously to a slightly pressurized insulin reservoir. Such a reservoir could be fastened under an adhesive strip, and could be changed at will, so its size could be very small. Placement of the reservoir on the abdomen would permit delivery of insulin, through the catheter, into the peritoneal space. The concept is illustrated in Fig. 21a.

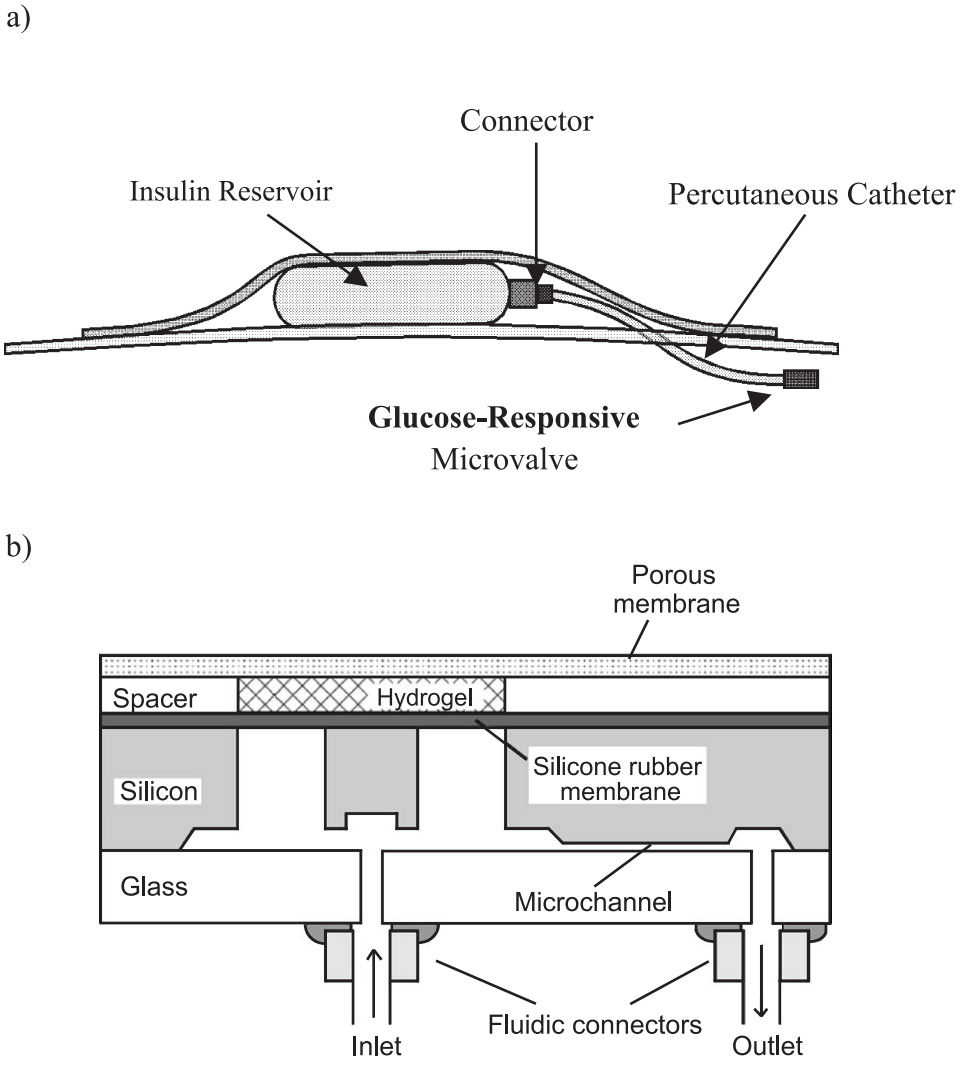

Fig. 21. (a) Concept of glucose-sensitive microvalve attached to the tip of a trancutaneous catheter leading from a pressured insulin reservoir. (b) Schematic of microvalve (reproduced with permission [38] © 2003 IEEE).

A schematic of the glucose-sensitive microvalve is provided in Fig. 21b. A glucose-sensitive hydrogel is sandwiched between a rigid but porous membrane that faces interstitial fluid, and an elastic diaphragm. The diaphragm separates the hydrogel from a flow channel whose inlet is connected to the insulin catheter. A solid embossment, or ''boss'', is attached to the diaphragm. This boss is positioned to close down on the flow inlet when the hydrogel expands, leading to changes in insulin flow.

Before describing the fabrication methods for this device, we note that this design minimizes some of the problems faced by devices based on hydrogels alone. First, the hydrogel is encased in a solid device, obviating problems surrounding mechanical integrity. Second, the hydrogel is isolated from both the insulin and the tissue in which the device is implanted. All biocompatibility issues are therefore shifted to the external MEMS materials, which can be coated with surfaces that retard protein fouling and tissue response [52,53]. Third, the small dimensions of the MEMS structures, including the hydrogel, suggest that rapid response is possible.

The fabrication process for the middle silicon part containing the elastic silicone rubber diaphragm and the flow restrictor is shown in Fig. 22. A 0.5-μm-thick thermal oxide is grown on both sides of a ⟨100⟩ single polished silicon wafer. The front-side (polished) oxide (bottom of Fig. 22a) is coated with photoresist and UV-patterned under a mask (Fig. 22.1). After development, the oxide is RIE-treated, and the result is an exposed region of crystalline silicon, surrounded by remaining oxide which serves as a mask for a subsequent KOH etch. The KOH etch defines the gap between the boss and the intake orifice, and also the microchannel connecting the intake to the output orifice (Figs. 22b). A deep reactive ion etching (DRIE) step, with mask shown in Fig. 22.2, is used to define the valve seat in the recess (Fig. 22c) A two-component silicone (PDMS) rubber is then spun onto the unpolished side of the silicon wafer (Fig. 22d) and cured, resulting in a 20-μm-thick layer. Finally, a second DRIE step, under the mask shown in Fig. 22.3, removes the silicon surrounding the central boss, leaving the boss ''hanging'' from a PDMS diaphragm (Fig. 22e). Fig. 23a shows the fabricated silicon part with the bossed diaphragm and the microchannel.

As before, the steps illustrated in Fig. 22 must be imagined in 3-D. The bottom oxide layer in Fig. 22a is actually patterned in 2-D according to the mask shown

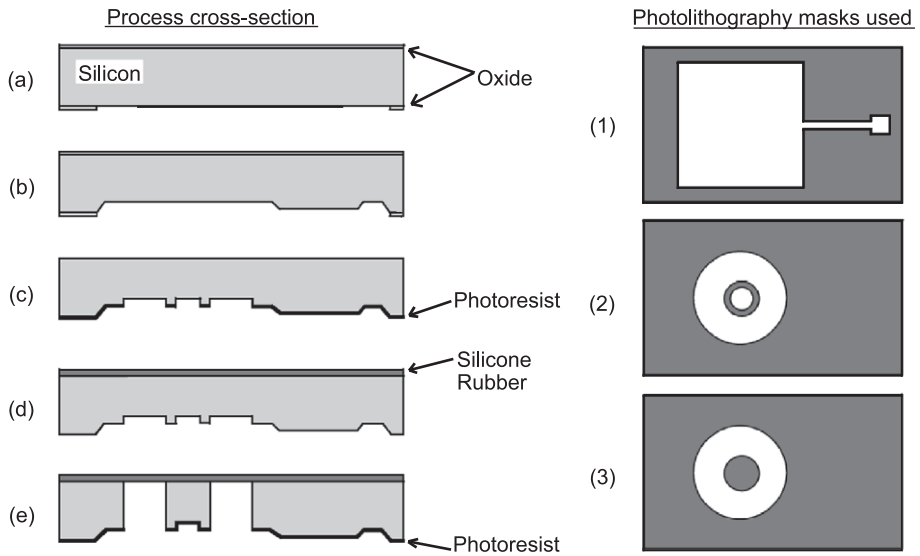

Fig. 22. Fabrication process for central, silicon-based part of the glucose-sensitive microvalve. (a) Oxide growth and patterning (Mask 1); (b) KOH etch (valve gap and V-shaped microchannel definition); (c) first deep RIE (valve seat definition, Mask 2); (d) silicone rubber spinning; (e) second deep RIE (membrane release and boss definition, Mask 3). Adapted with permission from Ref. [38] (© 2003 IEEE).

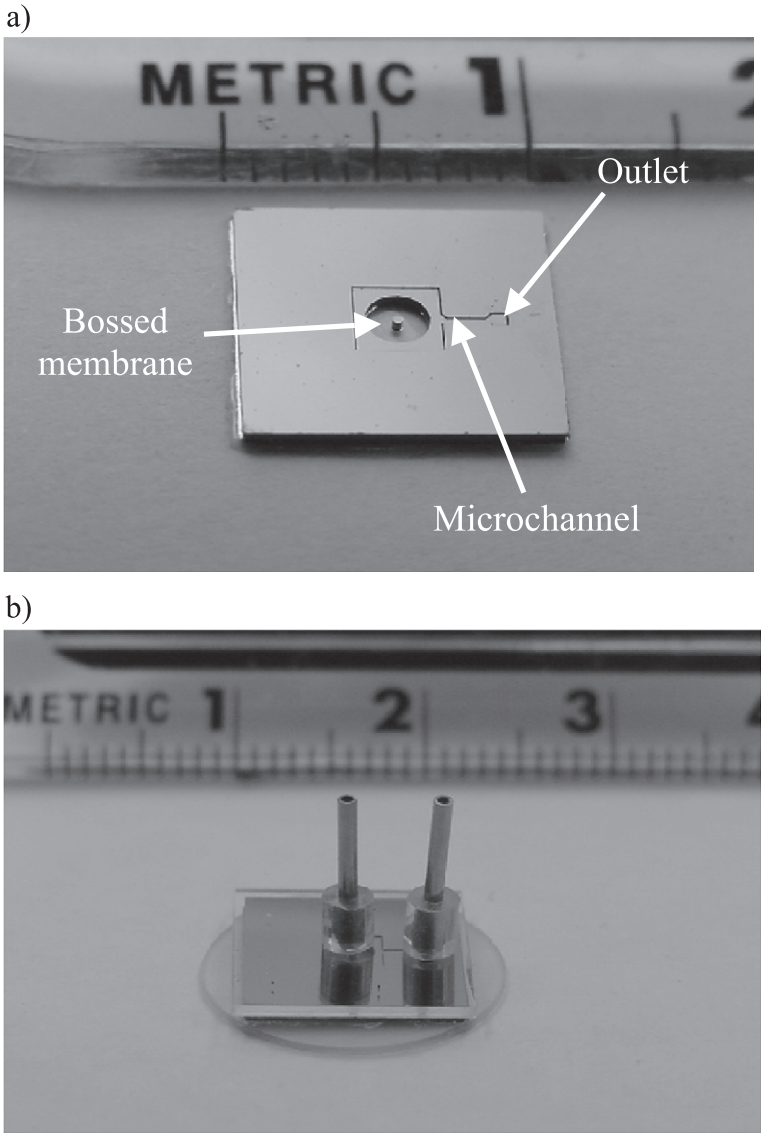

Fig. 23. (a) Central silicon piece, as prepared according to Fig. 22 (reproduced with permission from [38] (© 2003 IEEE)). (b) Assembled microvalve, inverted. Circular plate is Anopore® membrane. The silicon piece of panel (a) is seen through the transparent glass piece connected to the flow inlets and outlets. The PDMS spacer can be seen between the silicon piece and the circular plate. Reproduced with permission from Ref. [38] (© 2003 IEEE).

in Fig. 22.1. The oblong region defined by this mask for the flow channel is much narrower than either of the "square" regions, and the subsequent KOH etch in the flow channel region comes to a triangular vertex and stops, while the larger square regions form deeper basins. The partial depression illustrated in Fig. 22b–e therefore refers to a straight, narrow, "V"-grooved channel that is surrounded by unetched silicon. Finally, processes leading to the boss (Fig. 22c–e) have cylindrical symmetry, as can be gleaned from the circular shapes of the mask featured in Fig. 22.2,3.

To create an inlet and outlet to the valve, two orifices 250 μm in diameter are ultrasonically drilled into a Pyrex® glass substrate, which serves as inlet

and outlet orifices. The intake orifice in the glass plate and the diaphragm boss in the silicon substrate are aligned under an optical microscope and glued by a UV-curable epoxy.

A donut-shaped PDMS spacer layer is used as a washer into which the hydrogel is polymerized (Fig. 21). The bottom surface of this layer is activated in oxygen plasma and brought into bonding contact with the underlying PDMS diaphragm. In situ polymerization is then used to load the hydrogel into the microcavity defined by the washer, and the porous membrane is glued on top with a silicone adhesive. For experiments to be reported below, a nanoporous aluminum oxide (Anopore®, 100-nm diameter pores) was used. Fig. 23b is a photomicrograph of a completely assembled microvalve.

To render the microvalve glucose-sensitive, a hydrogel consisting of 18.4 mol% 3-methacrylamidophenylboronic acid (MPBA), 81.5 mol% acrylamide (AAm), and 0.1 mol% *N*,*N*′-methylene-bisacrylamide (Bis) is incorporated into the cavity between the porous membrane and the PDMS diaphragm. Free swelling studies of this hydrogel in PBS at pH 7.4 show a steady increase in swelling with increasing glucose concentration, as shown in Fig. 24a. This swelling behavior is due to stabilization of the charged, tetrahedral base form ($pK_a = 8.86$) of the phenylboronic acid moiety by complexation with glucose [42,43].

When the hydrogel is confined in the cavity, it is expected that an increased glucose level at pH 7.4 will lead to enhanced swelling pressure and downward distention of the elastic diaphragm, ultimately shutting off fluid flow. This prediction is borne out in experiments in which the microvalve, gravity-fed with water, is alternately immersed in PBS solutions containing glucose at concentrations 0 and 20 mM. As

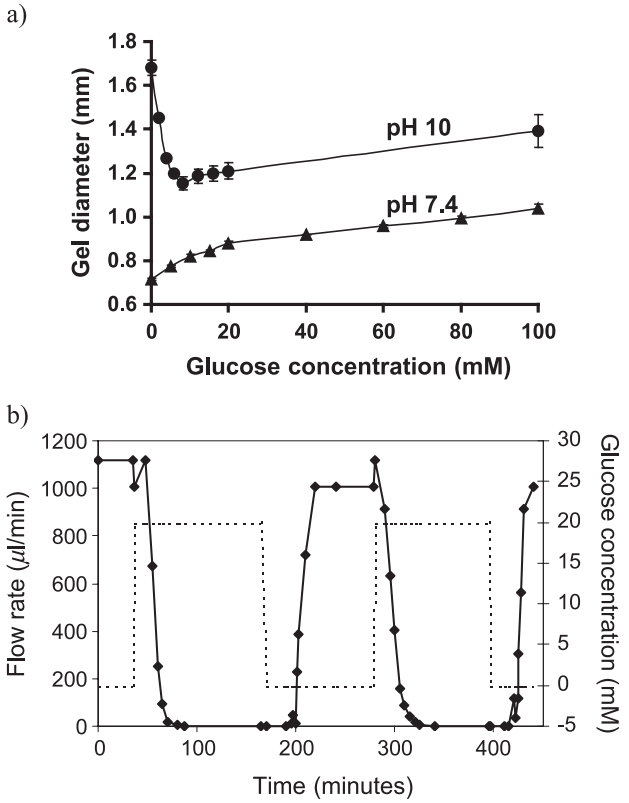

Fig. 24. (a) Glucose-dependent swelling and shrinking response of poly(MPBA-co-AAm) hydrogels at pH 7.4 and pH 10. (b) Reversible switch in flow rate (solid line) of fluid through microvalve containing this hydrogel, in response to changes in glucose concentration (dashed line) of an external phosphate-buffered saline solution at pH 7.4 (reproduced with permission from [38] (© 2003 IEEE)).

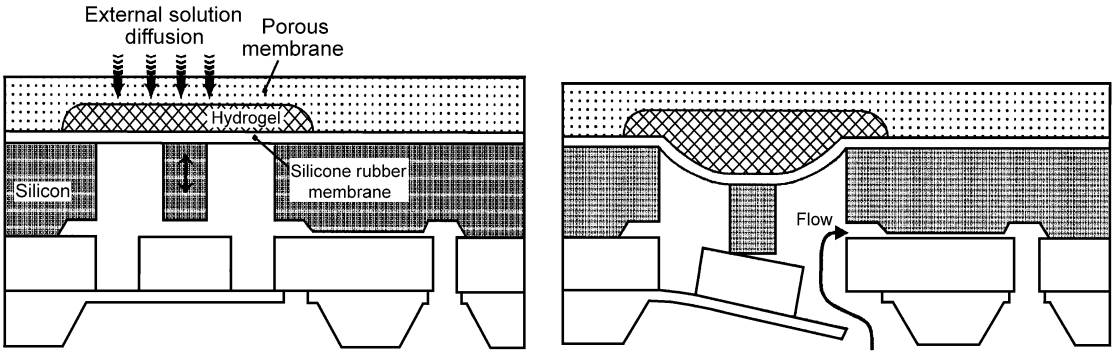

Fig. 25. Alternative scheme for microvalve in which swelling of hydrogel opens a gate for fluid flow and deswelling shuts the gate.

shown in Fig. 24b, a reversible switch between a "flow on" and a "flow off" state is effected about 20 min after change in glucose concentration. This response time may be improved in the future by altering characteristics of the porous membrane, the hydrogel, and the gap between the boss and the flow channel inlet.

An obvious deficiency in the present design is that the microvalve would shut off insulin flow response to increased glucose concentration, the opposite of the therapeutic goal. One might reverse the "polarity" of response by altering the MEMS component such that swelling of the hydrogel opens a gate for fluid flow. A simple scheme is shown in Fig. 25. Alternatively, one might redesign the hydrogel to shrink instead of swell with increasing glucose concentration. As shown in Fig. 24a, at pH 10, the MBPA-AAm hydrogels shrink and then reswell as glucose concentration increases. This behavior is due to reversible crosslinking of charged MPBA units on separate polymer chains by glucose [54]. At high glucose concentrations, these crosslinks are broken by competition from free glucose molecules. It is hoped that by suitable chemical alteration of the MPBA unit, the pK_a can be lowered such that shrinkage will occur with increasing glucose concentration over the desired range at physiological pH [55].

4. Conclusion

In this review, we have described various hard and soft microfabrication techniques that are available for the microfabrication of drug delivery devices. We have also described a suite of microfluidic devices that have be microfabricated in which flow is modulated by the swelling and shrinking of a hydrogel. Of these devices, the glucose-sensitive insulin delivery device is of the most interest for closed-loop drug delivery. Aside from the issues of response time and response polarity, it is worthwhile to consider the degree to which the latter device meets the ultimate goal of reproducing the function of a normal pancreas.

As pointed out by Steil et al. in this issue [56], the normal physiological response to a step increase in blood glucose concentration is a rapid initial pulse of insulin release followed by a ramp in secretion. This behavior would not be provided by the simple device described in this review, which has a simple on–off response. We conjecture, however, that more complex responses that more closely mimic those of the normal pancreas may be obtained in devices containing microfluidic circuits featuring series and parallel connections, fluid "capacitances", and different hydrogels controlling various parts of the microfluidic network. Work towards this end is underway.

Acknowledgements

This work was funded in part by grant DAMD17-02-1-0722 from the U.S. Army Medical Research and Materiel Command, and by grants from the Drug Delivery Center and Biomedical Engineering Institute at the University of Minnesota. We thank Paul Loftness, Sarah Hruby, Hao Hou, and David Beebe for their contributions and input.

References

[1] K.D. Wise (Ed.), Integrated sensors, microactuators, and microsystems (MEMS), Proc. IEEE 86 (1998) 1531–1746.
[2] A. Manz, H. Becker (Eds.), Microsystem Technology in Chemistry and Life Sciences, Springer, New York, 1999.
[3] J.M. Kohler, T. Mejevaia, H.P. Saluz (Eds.), Microsystem Technology: A Powerful Tool for Biomolecular Studies, Birkhauser, Boston, 1999.
[4] G.M. Whitesides, E. Ostuni, S. Takayama, X. Jiang, D.E. Ingber, Soft lithography in biology and biochemistry, Annu. Rev. Biomed. Eng. 3 (2001) 335–373.
[5] Cepheid, http://www.Cepheid.Com, 2003.
[6] R.S. Shawgo, A.C. Richards Grayson, Y. Li, M.J. Cima, Bio-MEMS for drug delivery, Curr. Opin. Solid State Mater. Sci. 6 (2002) 329–334.
[7] ChipRX. 2003. http://www.ChipRX.Com.
[8] Imedd. 2003. http://www.iMEDD.Com.
[9] B. Ziaie, J.A. VonArx, M.R. Dokmeci, K. Najafi, A hermetic glass silicon micropackage with high-density on-chip feedthroughs for sensors and actuators, J. Microelectromechanical Syst. 5 (1996) 166–179.
[10] S.A. Campbell, The Science and Engineering of Microelectronic Fabrication, Oxford Univ. Press, New York, 2001.
[11] C.J. Jaeger, Introduction to Microelectronic Fabrication, Prentice Hall, New Jersey, 2002.
[12] J.D. Plummer, M.D. Deal, P.B. Griffin, Silicon VLSI Technology, Prentice-Hall, New Jersey, 2000.
[13] M. Gad-El-Hak, The MEMS Handbook, CRC Press, Boca Raton, 2002.
[14] T.-R. Hsu, MEMS and Microsystems Design and Manufacture, McGraw Hill, New York, 2003.
[15] G.T.A. Kovacs, Micromachined Transducers Sourcebook, McGraw Hill, New York, 1998.
[16] P. Rai-Choudhury (Ed.), Handbook of Microlithography, Micromachining and Microfabrication, Micromachining and Microfabrication, vol. 2, SPIE, Bellingham, IEE, Washington, London, 1994.
[17] M.A. Schmidt, Wafer- to wafer bonding for microstructure formation, Proc. IEEE 86 (1998) 1575–1585.
[18] G.T.A. Kovacs, N.I. Maluf, K.A. Petersen, Bulk micromachining of silicon, Proc. IEEE 86 (1998) 1536–1551.
[19] H. Baltes, O. Paul, O. Brand, Micromachined thermally based cmos microsensors, Proc. IEEE 86 (1998) 1660–1678.
[20] N.C. Macdonald, SCREAM microelectromechanical systems, Microelectron. Eng. 32 (1996) 51–55.
[21] J.M. Bustillo, R.S. Muller, Surface micromachining for microelectromechanical systems, Proc. IEEE 86 (1998) 1552–1574.
[22] P.F. Van Kessel, L.J. Hornbeck, R.E. Meier, M.R. Douglass, A MEMS-based projection display, Proc. IEEE 86 (1998) 1687–1704.
[23] J.A. Geen, S.J. Sherman, J.F. Chang, S.R. Lewis, Single-chip surface micromachined integrated gyroscope with 50 degrees/hour root Allan variance, IEEE J. Solid-State Circuits 37 (2002) 1860–1866.
[24] H. Guckel, High-aspect-ratio micromachining via deep X-ray lithography, Proc. IEEE 86 (1998) 1586–1593.
[25] K.Y. Lee, N. Labianca, S.A. Rishton, S. Zolgharnain, J.D. Gelorme, J. Shaw, T.H.P. Chang, Micromachining applications of a high resolution ultra-thick photoresist, J. Vac. Sci. Tech., B 13 (1995) 3012–3016.
[26] K. Roberts, F. Williamson, G. Cibuzar, L. Thomas, The fabrication of an array of microcavities utilizing SU-8 photoresist as an alternative 'LIGA' technology, Proc. Thirteenth Biennial Univ/Gov/Ind Microelectronics Symp (IEEE), 1999, pp. 139–141.
[27] G.M. Whitesides, A.D. Strook, Flexible methods for microfluidics, Phys. Today 54 (2001) 42–48.
[28] S.R. Quake, A. Scherer, From micro- to nanofabrication with soft material, Science 290 (2000) 1526–1540.
[29] H. Becker, U. Heim, Silicon as tool material for polymer hot embossing, (1999) 228–231.
[30] G.B. Lee, S.C. Chen, G.R. Huang, W.C. Sung, Y.H. Lin, Microfabricated plastic chips by hot embossing methods and their applications for DNS separation and detection, Sens. Actuators, B 75 (2001) 142–148.
[31] H.S. Lee, S.K. Lee, T.H. Kwon, S.S. Lee, Microlens Array Fabrication by Hot Embossing Process, Proc. IEEE/LEOS Optical MEMS Conf., 2002, pp. 73–74.
[32] D.J. Beebe, J.S. Moore, Q. Liu, R.H. Liu, B.-H. Devadoss, Microfluidic tectonics: a comprehensive construction platform for microfluidic systems, Proc. Natl. Acad. Sci. 97 (2000) 13488–13493.
[33] D.T. Eddington, D.J. Beebe, Flow control with hydrogels, Adv. Drug Delivery Revs. (this issue).
[34] Y. Gu, A. Dhanarajan, R.A. Siegel, A hydrogel-incorporated crosscut configuration for rhythmic, pulsatile flow control, Proc. 30th Ann. Meet. Exp. Controlled Release Society, 2003, Glasgow, Scotland.
[35] Y. Hirokawa, T. Tanaka, Volume phase transition in a nonionic gel, J. Chem. Phys. 81 (1984) 6379–6380.
[36] H. Inomata, S. Goto, S. Saito, Phase transition of n-substituted acrylamide gels, Macromolecules 23 (1990) 4887–4888.
[37] Y. Gu, A. Baldi, M. Lei, B. Ziaie, R.A. Siegel, A microfabricated, hydrogel-loaded tethered valve for active flow control, Proc. 30th Ann. Meet. Exp. Controlled Release Society, 2003, Glasgow, Scotland.
[38] A. Baldi, Y. Gu, P. Loftness, R.A. Siegel, B. Ziaie, A hydrogel-actuated environmentally-sensitive microvalve for active flow control, J. Microelectromechanical Syst. 12 (2003) 613–621.
[39] J. Kost, T.A. Horbett, B.D. Ratner, M. Singh, Glucose-sensitive membranes containing glucose oxidase: swelling, activity, and permeability studies, J. Biomed. Mater. Res. 19 (1985) 1117–1122.
[40] K. Ishihara, K. Matsui, Glucose-responsive insulin release from polymer capsule, J. Polym. Sci., Polym. Lett. 24 (1986) 413–417.
[41] C.M. Hassan, F.J. Doyle Ii, N.A. Peppas, Dynamic behavior of glucose-responsive poly(methacrylic acid-*g*-ethylene glycol) hydrogels, Macromolecules 30 (1997) 6166–6173.
[42] K. Kataoka, H. Miyazaki, T. Okano, Y. Sakurai, Sensitive

glucose-induced change of the lower critical solution temperature of poly[*n*,*n*-dimethylacrylamide-co-(3-acrylamidophenylboronic acid] in physiological saline, Macromolecules 27 (1994) 1061–1062.

[43] K. Kataoka, H. Miyazaki, M. Bunya, T. Okano, Y. Sakurai, Totally synthetic polymer gels responding to external glucose concentration: their preparation and application to on–off regulation of insulin release, J. Am. Chem. Soc. 120 (1998) 12694–12695.

[44] R.A. Siegel, B.A. Firestone, Mechanochemical approaches to self-regulating insulin pump design, J. Control. Release 11 (1990) 181–192.

[45] M.J. Taylor, S. Tanna, P.M. Taylor, G. Adams, The delivery of insulin from aqueous and nonaqueous reservoirs governed by a glucose-sensitive gel membrane, J. Drug Target. 3 (1995) 209–216.

[46] A.A. Obaidat, K. Park, Characterization of protein release through glucose-sensitive hydrogel membranes, Biomaterials 18 (1997) 801–806.

[47] G. Albin, T.A. Horbett, S.R. Miller, N.L. Ricker, Theoretical and experimental studies of glucose sensitive membranes, J. Control. Release 7 (1987) 267–291.

[48] P.E. Grimshaw, J.H. Nussbaum, A.J. Grodzinsky, D.M. Yarmush, Kinetics of electrically and chemically induced swelling of polyelectrolyte gels, J. Chem. Phys. 93 (1990) 4462–4472.

[49] A. English, T. Tanaka, E.R. Edelman, Equilibrium and non-equilibrium phase transitions in copolymer polyelectrolyte hydrogels, J. Chem. Phys. 107 (1997) 1645–1654.

[50] R.J. Phillips, A hydrodynamic model for hindered diffusion of proteins and micelles in hydrogels, Biophys. J. 79 (2000) 3350–3354.

[51] B. Amsden, Diffusion in polyelectrolyte hydrogels: application of an obstruction-scaling model to solute diffusion in calcium alginate, Macromolecules 34 (2001) 1430–1435.

[52] M. Zhang, M. Ferrari, Hemocompatible polyethylene glycol films on silicon, J. Biomed. Microdev. 1 (1998) 81–89.

[53] T. Desai, D. Hansford, M. Ferrari, Micromachined interfaces: new approaches in cell immunoisolation and biomolecular separation, Biomol. Eng. 17 (2000) 23–36.

[54] Y. Gu, R.A. Siegel, Studies of the Equilibrium Swelling Response of Hydrogels Containing Phenylboronic Acid Moieties, Proc. 29th Ann. Mtg. Controlled Release Soc., Seoul, Korea.

[55] Y. Gu, Swelling properties of phenylboronic acid-containing hydrogels and their application in microfluidic drug delivery devices, PhD Thesis, University of Minnesota, 2003.

[56] G.M. Steil, A.E. Panteleon, K. Rebrin, Closed-loop insulin delivery—the path to physiological glucose control, Adv. Drug Deliv. Rev. 56 (2003) 125–144 (this issue)

[57] A. Baldi, B. Ziaie, Introduction to micro and nanofabrication, in: B. Bushan (Ed.), Springer Handbook of Nanotechnology, Springer, Berlin. (in press).